2012

Role of Cardiac Troponin I's Carboxy Terminus in Regulating Cardiac Contraction

Nancy Meyer

THE FLORIDA STATE UNIVERSITY

COLLEGE OF ARTS AND SCIENCES

ROLE OF CARDIAC TROPONIN I'S CARBOXY TERMINUS IN REGULATING CARDIAC CONTRACTION

By

NANCY MEYER

A Thesis submitted to the
Department of Biological Science
in partial fulfillment of the
requirements for the degree of
Master of Science

Degree Awarded:
Summer Semester, 2012

Nancy Meyer defended this thesis on April 17th, 2012.

The members of the supervisory committee were:

P. Bryant Chase
Professor Directing Thesis

Kenneth Taylor
Committee Chair

Piotr Fajer
Committee Member

The Graduate School has verified and approved the above-named committee members, and certifies that the thesis has been approved in accordance with university requirements.

ACKNOWLEDGEMENTS

First I must thank my advisor Dr. Bryant Chase for his guidance and support. I would also like to thank my labs' current and past members. Thank you also to Rani Dhanarajan and Margaret Seavy in the Biology Department at FSU, as teachers and without whom this work would not have progressed.

My acknowledgements of course go to my committee members, both current and past: Ken Taylor, Piotr Fajer, Stephan von Molnar and Linda Hirst of the Physics Department, and Lei Zhu of Chemistry, who each had valuable contributions to my work and whose advice contributes still to my work now – thanks for your implicit confidence. Thank you, too, to Michael Chapman, for giving me the chance to stay in research, and for employing me while I write this!

Especially I would like to thank Campion Loong and Gregg Hoffman for their scientific advice, support, and friendship. Much gratitude goes, too, to Kerri Maddox for her support (both moral and administrative!) as well as that of Joan Hare in the IMB. And special thanks to Aya Kataoka, Myriam Badr, Brenda Schoffstall, and Nicolas Brunet for all the generous help and guidance they provided me. They were really an exceptional team to work with.

And to Omar, who has helped me keep going. Yay!

TABLE OF CONTENTS

LIST OF TABLES

LIST OF FIGURES

ABSTRACT

Normal cardiac function involves the highly regulated switching of contraction on and off by Ca^{2+}-dependent conformational changes in the troponin-tropomyosin complex. A myriad of factors, both biochemical and mechanical, adaptively modulate the regular systole-diastole transition, though all ultimately act through the proteins of the sarcomere. Among the most influential is the ternary troponin complex, lesions of which account for the etiology of a number of cardiomyopathies, including dilated cardiomyopathy, familial hypertrophic cardiomyopathy, and myocardial stunning. The latter can often be traced in particular to dysfunction of cardiac troponin I, the "inhibitory" subunit, which is key to the on/off movements of tropomyosin on the thin filament. This research examines the Ca^{2+}-dependent regulatory role of cardiac troponin I's C-terminus *in vitro,* as well as its development as a clinical marker for use in SnO_2 nanobelt FET biosensors.

Investigations into how cardiac troponin I's C-terminal mobile domain and adjacent regions contribute to the Ca^{2+}-dependent "switch" were conducted using the *in vitro* motility assay. Specifically, we test the hypothesis that cTnI's mobile domain is tightly-coupled to the so-called switch peptide domain, to which it is immediately adjacent in the primary sequence. The ability of wild-type cardiac troponin complexes to regulate filament sliding was compared to that of complexes containing one of two mutant cardiac troponin Is: a C-terminally truncated cardiac troponin I lacking the mobile domain, and a cardiac troponin I that incorporated an 8-residue flexible linker between the switch peptide and mobile domain.

We find that neither mutation affected maximum filament sliding speeds, indicating that neither the mobile domain nor its adjacency to the switch peptide are required for full activation in the presence of Ca^{2+}. Each mutant complex was found to increase the Ca^{2+}-sensitivity of activation, presumably in different ways. Cooperativity coefficients decreased with each compared to wild type, which agrees with a more permissive range of motion for the switch peptide (i.e. a more ready association with the N-lobe of troponin C) in which fewer activated regulatory units are required to effect the same activating level of crossbridge association. The truncated troponin I complex also failed to fully inhibit filament sliding at low $[Ca^{2+}]$, showing that while the mobile domain is necessary for full Ca^{2+}-dependent inhibition, some inhibitory interaction with actin-tropomyosin remains.

These efforts have been timely because, with increasing structural data, it has recently become possible to test detailed hypotheses about the functional role of the of cardiac troponin I C-terminus in Ca^{2+} regulation of thin filaments. It has also been of clinical importance to optimize point-of-care troponin I biosensor devices for the rapid and reliable detection of this myocardial infarction marker.

CHAPTER 1

INTRODUCTION

Even the most recent publications about troponin's role in contractile Ca^{2+} regulation will refer to the "poorly understood" function of the cardiac troponin I C-terminus. However, an increased focus on the structure and associations of this protein region in recent years has improved our understanding of how this subdomain of cTnI and its adjacent regions contribute to Ca^{2+} control of cardiac muscle contraction. While the regulatory function of cTnI's C-terminus may not yet be fully understood, the work that follows was initially undertaken when it was even less so.

The research presented here examines the relationship between Ca^{2+} regulation of cardiac contractility and the involvement of cardiac troponin I's extreme C-terminal mobile domain (Md). Troponin I (TnI) is a key element in regulating activation in striated muscles, and is thus central to the control of cardiac and skeletal muscle contraction (its isoforms referred to as cTnI and sTnI, respectively). TnI is regarded as the inhibitory subunit of the ternary troponin complex, which modulates Tm's position on the thin filament in a Ca^{2+}-dependent manner. As mentioned, the mechanism by which its C-terminal regions cooperate as a Ca^{2+}-dependent "switch" is not fully understood and the potentially significant role of TnI's Md in this mechanism warranted further investigation. Of clinical interest, over 25 genetic mutations in the cTnI gene (TNNI3) have been implicated in the pathogenesis of familial hypertrophic cardiomyopathy (FHC), more than 18 of which occur within the cTnI C-terminus [1-4], and the following study builds upon the lab's previous research in this area [5-9].

1.1 Sarcomere Structure

A molecular description of striated muscle contraction begins with the sarcomere. Both skeletal and cardiac vertebrate muscle owe the name "striated" to their visibly well-ordered sarcomeric arrays and the proteins therein. Through a light microscope we can distinguish some of the major protein components of the basic contractile unit, generally grouped as those of the Z-discs, which "bookend" each sarcomere, and those that lie lengthwise normal to the Z-discs: the thin filaments, thick filaments, titin, and nebulin/nebulette. Actin-based thin filaments

anchored in the Z-discs extend out, rod-like, from either boundary toward the center of the sarcomere, providing a foundation for the ratchet-like process of contraction (Fig. 1c and 4). It is along the thin filaments that Tn complexes exert their effect. The varying overlap of thick and thin filaments generate the characteristic banding visible within sarcomeres. In particular, the I-bands that are located to the inside of each Z-disc are zones of thin filaments not superimposed by thick filaments. The A-band comprises the full length of thick filaments and appears generally darker where overlapping with the thin filaments. The lighter, central H-zone represents thick filaments not superimposed by thin filaments from either side (Figs 1b). Note the multitude of these end-to-end sarcomeric units, comprising one myofibril, that are arrayed lenthwise within the sarcolemmal membrane of a single muscle cell, or myofiber. In contrast to the skeletal muscle fiber depicted in Figure 1a, cardiac myocytes generally possess one or at most two central nuclei and their branching morphology promotes interdigitation of cells.

Working myocytes, both cardiac and skeletal, require a dense packing of mitochondria proximal to the myofibrils and an intimate wrapping of the sarcoplamic reticulum (SR). These structures, respectively, generate the high ATP supply required by contracting myofibers, and serve as local Ca^{2+} reservoirs. In response to depolarization, the SR releases its Ca^{2+} stores into the cytoplasm to initiate contraction, and then resequesters the cations to effect relaxation.

In detail, the coordinated contraction and relaxation requires sophisticated regulatory machinery capable of responding to the Ca^{2+} fluxes from which the "on/off" signal derives. We will first address the characteristics and arrangement of the primary sarcomeric proteins, before discussing in detail the mechanism of contraction and Ca^{2+} regulation. We will then narrow our focus to the role of cardiac TnI (cTnI) and experiments to investigate the regulatory function of cTnI's C-terminus.

1.1.1 Myosin and the Thick Filament – Powering Contraction

The myosin family of motor proteins is now classified into ~35 subfamilies based on sequence, and it is suggested that most eukaryotic cells express over a dozen different isoforms spread over these groups [10]. Myosins represent a wide range of structural, mechanical, and kinetic properties tailoring each to a specific cellular task from motility and transport to the sensing of cellular mechanical forces. The major motor protein of muscle is myosin II, and it shares its family's signature biochemical characteristic of converting the energy of ATP hydrolysis into force and movement through a cyclical interaction with the actin filament [10]. In

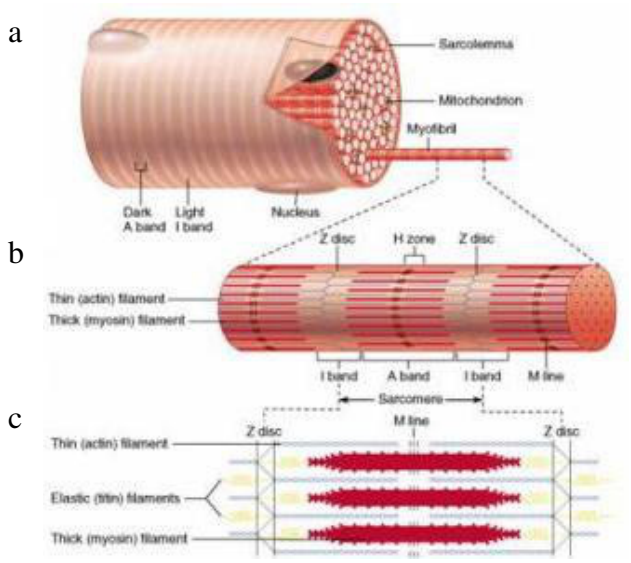

Figure 1. Skeletal muscle myofiber structure. (a) Cell cross-section, (b) individual myofibril, and (c) a single sarcomer unit (~2.5 nm in length). Structures in panels b and c also apply to cardiac muscle. (Copyright © 2001 Benjamin Cummings, an imprint of Addison Wesley Longman, Inc.)

the case of myosin II, binding to actin and subsequent ATP hydrolysis cause the conformational changes that effectively "pull" thick and thin filaments past one another in a ratchet-like fashion to longitudinally contract sarcomeres (Fig. 4). Collectively, this results in overall muscle contraction: the flex of a bicep, the squeeze of a ventricle.

Myosin II, like its relatives, comprises three structural domains of different function: the head, neck, and tail domains, as illustrated in Figure 4a. A single myosin II molecule is made up of six polypeptides: two myosin heavy chains (MHC) and four light chains (MLC). Each MHC is associated with two MLCs, one essential light chain (ELC) and one regulatory (RLC), that bind to each MHC's neck region. There are two isoforms of the skeletal muscle ELC, coded for by the same gene, which differ at the N-terminus. Ventricular and atrial cardiac tissues express their own unique MLC isoforms, designated VLC-1 and ALC-1, respectively [11]. The paired MHC tails form a coiled-coil, and it is the coiled-coils from each MHC pair which bundle tightly to assemble into the thick filament backbone.

For experimental purposes, rabbit skeletal myosin II can be cleaved proteolytically into various fragments (Fig. 4b). Both subfragment 1 (S1) and heavy meromyosin (HMM) are commonly used soluble fragments which are prepared by papain treatment or mild chymotryptic digestion, respectively. Both S1 and HMM retain actin-binding and actin-activated MgATPase activities. Papain cleavage results in removal of the tail domains, disassociating the MHCs and

leaving an ~110 kD S1 composed of a single motor domain and its neck-associated light chains (LCs). Mild chymotrypsin treatment in the presence of Mg^{2+}, on the other hand, leaves intact two associated heads and necks (including LCs) and a short length of coiled-coil tail, constituting the ~350 kD HMM which will be used in this study's *in vitro* motility assays (Chapter 2).

The MHC globular motor head comprises a 25kD N-terminal subdomain (gray, below ATP-binding site in Fig. 2), upper and lower 50kD subdomains (as indicated, Fig. 2) and the C-terminal converter subdomain (aqua, Fig. 2). Within the motor head lie two important binding sites, that of ATP and actin. Actin binding occurs at two distinct subsites and is mediated by closure or opening of the flexible cleft region present between the upper and lower 50 kD subdomains [12]. The binding pocket for ATP is the catalytic active site of ATP hydrolysis. Structural "snapshots" and EPR studies in solution, with and without bound nucleotide, indicate that the open and closed conformations of the cleft region are strongly coupled to actin binding and occupancy of the nucleotide binding site, i.e., presence of ATP in the binding pocket opens the cleft or "jaw" region, decreasing actin affinity from nM to mM and allowing actomyosin dissociation [12, 13]. Closing of the cleft region upon ATP hydrolysis allows weak binding to actin and the subsequent release of P_i is then coupled with strong binding to the thin filament as will be illustrated in discussion of the crossbridge cycle (Section 1.1.4).

Typically >300 asymmetric myosin II molecules assemble to form a thick filament of around 1.6 μm in length and ~18 nm in thickness [14, 15]. The giant protein titin (3,000 kD) elastically anchors the thick filaments to the z-disks while providing a more rigid support within the A-band. Also localized to "stripes" within the crossbridge-containing region of thick filaments is the ~130 kD myosin binding protein C (MyBP-C). It is known to link myosin rods to titin near the center of the A-band, but also plays a role in contractile regulation. Phosphorylation releases MyBP-C's N-terminus from association with the S2 portion of myosin (Fig. 4), which can otherwise slow cross-bridge cycling rates and promote relaxation. [16]. MyBP-C has also recently been shown to interact directly with actin in intact skeletal muscle [17]. Interestingly, cardiac MyBP-C (cMyBP-C) is the site of over 72 mutations associated with familial hypertrophic cardiomyopathy (FHC), of particular interest to our lab owing to the number of FHC-related mutations associated with cTnI's C-terminus. This is second only to the number found in the cardiac β-myosin heavy chain (βMyHC).

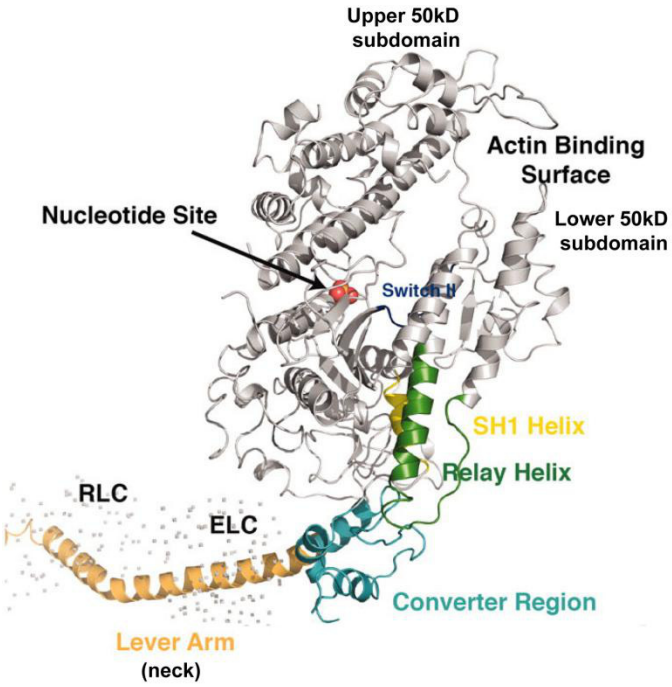

Figure 2. Ribbon representation of myosin II head and neck. Crystal structure of adult chicken muscle myosin S1, PDB ID 2MYS. Light chains not fully depicted here. (Adapted from Houdusse and Sweeney, 2001.)

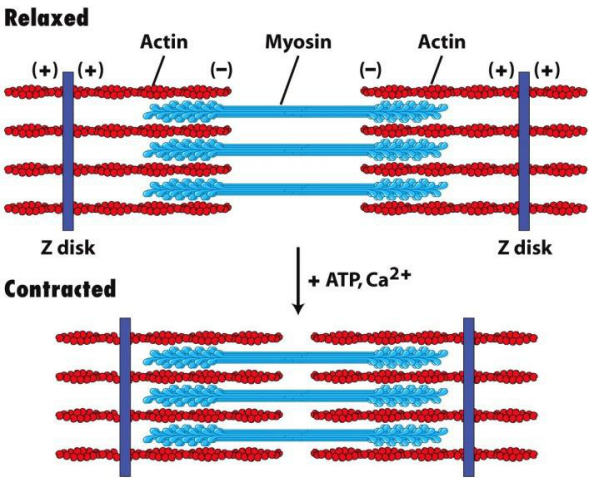

Figure 3. Arrangement of thin and thick filaments within a sarcomere. Individual myosin heads ratchet toward actin (+) ends, collectively pulling z-disks closer during contraction (bottom) (Lodish, Molecular Cell Biology, 6th Edition, 2008.).

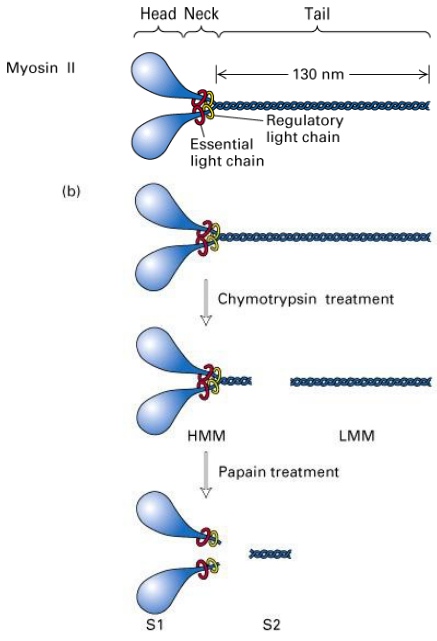

Figure 4. Myosin II molecule (a) and its major proteolytic subfragments (b). (Lodish, Molecular Cell Biology, 4th Edition, 2001.)

1.1.2 Thin Filament and Regulatory Proteins

1.1.2.1 Actin and tropomyosin. The major structural component of the thin filament is F-actin (*F* for "filamentous"). Strands of F-actin form by the end-to-end association of polar globular G-actin monomers (42 kDa) in the presence of ATP. Each thin filament (~ 6-7 nm diameter) contains two such long-pitch, right-handed helices coiled about one another, which then associate with the regulatory proteins troponin and tropomyosin, as seen in Figure 6. Of six uniquely-encoded actin isoforms found in mammals, α-cardiac (*ACTC*) and α-skeletal (*ACTA1*) actin are differentially co-expressed in normal myocardium. They possess high sequence-similarity and it is α-skeletal actin mRNA which predominates by adulthood in human hearts [18]. (The two others occur in non-muscle cytoplasm and two primarily in smooth muscle) [19, 20]. Each monomer contains four structural domains and it is in a cleft between the major two that are found nucleotide and divalent ion (Mg^{2+}) binding site. A binding site also exists for the catalytic head region of thick filament myosin; it is the enhanced rate of ATP hydrolysis by the myosin head upon binding the thin filament that is coupled to the conformational changes responsible for contraction.

Encircling the length of each F-actin filament are two chains of the heterodimeric protein tropomyosin (Tm). Each tropomyosin molecule (~33 kDa) is composed of two α-helical chains arranged as a coiled-coil, consisting, in striated muscle, of a ratio of α and β isoforms that is dependent upon developmental stage and fiber type [19]. Cardiac muscle possesses almost exclusively the α-Tm homodimer. Each Tm dimer binds cooperatively head-to-tail with a 8-11 residue overlap to fill lengthwise the two grooves of the actin filament. Each molecule spans about seven actin monomers (i.e. one Tm dimer spans a single half-helical turn of the thin

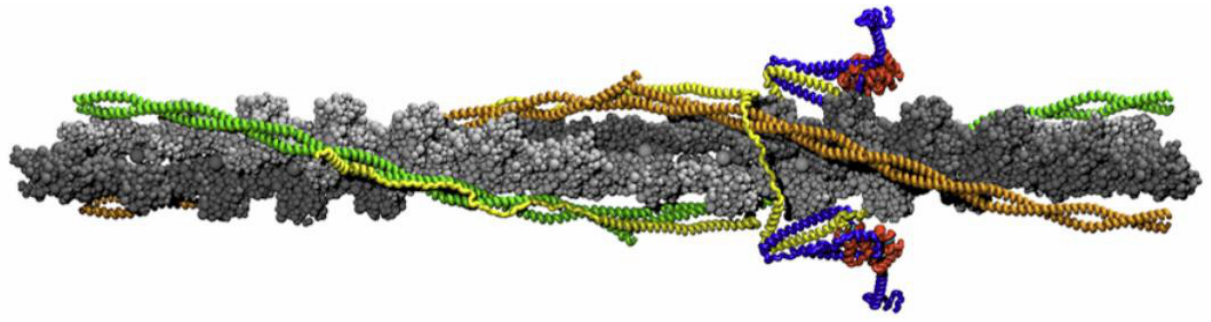

Figure 5. Thin filament and regulatory proteins, Tn and Tm. Model of an actin filament (grays) encircled by ribbon diagrams of two molecules of Tm (green and orange) showing two associated Tn complexes: TnI in blue, TnC (red), and TnT (yellow). (Tardiff, 2011)

filament). One role of tropomyosin is to increase the stiffness of the thin filament and aid in its stabilization by inhibiting polymerization-depolymerization. Its more dynamic role is its regulatory duet with troponin (Tn), acting together as a calcium-sensitive switch to turn on and off actomyosin crossbridge formation [19]. FHC mutations in α-tropomyosin (V95A, D175N, E180G) have been found to enhance regulated actin filament sliding at sub-saturating Ca^{2+}, i.e. increase Ca^{2+} sensitivity [21]. We will restrict further discussion to cardiac-specific homodimeric α-Tm.

1.1.2.2 Troponin complex. The three subunits of Tn are troponin C (TnC, the Ca^{2+}-binding subunit), troponin I (the inhibitory subunit), and troponin T (TnT, the major Tm-binding subunit). The ~34 kD TnT binds Tm and TnI with the main binding sites divided between TnT's N-terminal and C-terminal portions, TnT1 and TnT2, respectively [22-25]. It is the "glue" that holds the complex in place along the thin filament at intervals equivalent to seven actin monomers (an actin-Tn-Tm ratio of 7:1:1). The far C-terminus TnT2 interacts with TnI-TnC and Tm [26], while TnT2 residues 226-270 (TnT helix 2) form a coiled-coil structure with helix 2 of TnI (constituting the IT-arm). Recent H/D exchange mass spectrosopy corroborates evidence of the IT-arm being the most stable part of the Tn complex [27, 28]. These regions are illustrated in Figures 9 and 10. TnT1, at TnT's N-terminus, associates with the C-terminus of Tm as well as an overlapping region with the neighboring Tm N-terminus (seen in Fig. 5 as well as 10). Here it presumably has some influence on the flexibility and thus the equilibrium position of Tm, which is a crucial factor in contractile regulation.

TnC is the Ca^{2+}-sensing subunit, a member of the calmodulin superfamily of structurally-related Ca^{2+}-signalling proteins. It is ~18 kD and, corresponding to its roughly dumbell-shaped appearance in ribbon models (red in Figs. 8 and 9), it can be divided into two main globular domains, the N- and C-lobes. Divalent cation binding sites III and IV in the C-lobe of both cardiac and skeletal TnC are considered to serve structurally; they are high affinity sites and normally occupied by Mg^{2+} under relaxing conditions (~100 nM Ca^{2+}). The C-lobe of TnC is thought to hold fast to an N-terminal segment of TnI independently of [Ca^{2+}]. The regulatory N-lobe contains binding site II (and also a site I in sTnC only); both possess lower metal binding affinity, but high Ca^{2+}-selectivity. Calcium binding to this site(s) induces structural changes in both TnC isoforms. On the basis of early crystal structures of sTnC [29, 30], it was proposed that Ca^{2+} binding to the N-lobe results in an "open" conformation, which exposes a hydrophobic

pocket capable of binding to TnI. This is seen in Figure 7 as a repositioning of helix B and C relative to helix D. This hydrophobic pocket "opening" is the basis for important interactions between TnI and TnC that are discussed further below.

Cardiac TnI is the ~24 kD inhibitory subunit which differs from the skeletal isoform in that it possesses an additional 32 cardiac-specific residues at its N-terminus. As mentioned, its helix 2 serves to rigidly associate TnI with TnT via formation of an alpha-helical coiled-coil, and other portions of TnT in turn act as an anchor of the Tn complex to the thin filament. The switch (Sp) domain (switch helix) of TnI binds to the hydrophobic pocket in the N-lobe of TnC only in the presence of Ca^{2+}, and is associated with actin at low Ca^{2+} [31]. The inhibitory peptide (Ip), lies N-terminally adjacent to the Sp in the primary sequence and is largely composed of basic amino acids which bind tightly to both cTnC and actin, though not simultaneously [32]. In complex, TnI's C-terminal mobile (Md) domain also appears to bind actin at low, but not high Ca^{2+} [31, 33, 34], as depicted in Figure 10. Its position and possible secondary structure in the presence of Ca^{2+} is debated and may be key to understanding potential activation-enhancing interactions with other Tn components [31, 35]. High flexibility characterizes the sTnI "mobile" domain in solution (in complex), as this domain is "NMR-visible", whereas the rest of the Tn complex is not with NMR studies, indicating little secondary structure independent of Ca^{2+} [33, 35]. Contrast this with evidence that suggests the C-terminus more broadly is intrinsically folded in the Ca^{2+}-saturated state [33, 36]. The TnI N-terminal regions, for their part, are expected to play a critical role in ATPase activation (specifically skeletal residues ~ 57-96) [37].

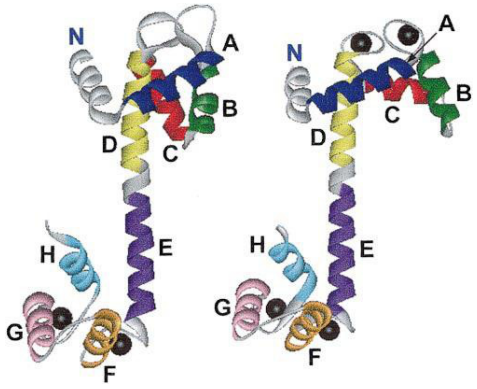

Figure 6. sTnC structure in the absence (left) and presence (right) of Ca^{2+}. Helices are labeled from A-H. Note B and C helix movement relative to D. Occupancy of sites I and II as shown as black spheres in the N-lobe (top) (Gordon, 2000, from the work of Herzberg et al. and Sundaralingam et al.)

Much of what we know about the complex's conformational response to Ca^{2+} comes from static structure analysis; before and after, so to speak. Two foundational sources are the crystal structures of Vinagradova and co-workers in 2005 and Takeda and co-workers in 2003 [24, 25]. Vinogradova et al. provide the sTn core with and without Ca^{2+}; Takeda et al. provide that of cTn, but only in the presence of Ca^{2+} (Figs. 9 and 10). Atomic structure determinations of the Tn core has often been limited to the subunit fragments that are amenable to crystallization as a complex. For example, while a full sTnI (residues 1-182) was included in the Ca^{2+}-bound complex, Vinagradova et al. incorporated only sTnI-(1-137) in the Ca^{2+} crystal. Similarly, only one Ca^{2+}-bound structure from Takeda et al. included the cTnI Md, and neither included the cardiac-specific N-terminus. In cases where the TnI C-terminus was included, the Md nonetheless was not represented by electron density, presumably due to high flexibility or presence of multiple conformers. The structures of both groups approach reasonable atomic resolution and can suggest some evidence of isoform-specific differences, however high B-factors in each may hint at a predisposition for the very dynamics we hope to understand.

As attempts to crystallize the entirety of Tn have faced challenges, similarly, we might not expect to crystallize as variable a complex as the thin filament at any level of decoration. Information about Tn's Ca^{2+}-dependent position on the thin filament comes largely from electron microscopy (EM). EM reconstructions support the Ca^{2+}-dependent shifting of Tn from the inner to outer domain of actin [38] and that it is Tm's equilibrium position about the actin filament that is shifted in response to Ca^{2+} binding to Tn [34]. Importantly, docking of the Md model onto a cryo-EM density map of thin filament at low Ca^{2+}, and subsequent placement of the entire Tn regulatory head region, supported a Tn electrostatic interaction with actin and suggested the "pushing" of Tm by Tn's coiled-coil to achieve relaxation [33]. This was further corroborated by additional EM in which thin filaments were labeled with an engineered construct representing C-terminal TnI in the effort to resolve where Tn is anchored on actin-tropomyosin [31]. More recently, a cTn complex incorporating a $cTnI_{1-192}$ truncation mutant was shown to perturb the equilibrium position of Tm on the thin filament in the presence of Ca^{2+} toward an "enhanced high Ca^{2+}-state"(C-state) [39]. That is, removal of 17 C-terminal residues from cTnI appears to bias Tm's position toward exposing more of actin's myosin binding site than WT Ca^{2+}-bound cTn permits. While $cTnI_{1-192}$ alone (no cTnT or cTnC) is able to bind actin and actin:Tm with the same affinity as WT cTnI, the mutant $cTnI_{1-192}$ complex is nonetheless unable to fully inhibit

ATPase activity in the absence of Ca^{2+} [40]. Further evidence of cTnI's C-terminal regulatory importance is discussed in Section 1.4.

1.2 E-C Coupling, Crossbridge Cycling, and Myofilament Activation

1.2.1 Excitation-contraction coupling in striated muscle

Excitation-contraction coupling refers to the process by which electrochemical action potentials trigger myocytes to contract via sequential cell membrane depolarization and rise in cytoplasmic [Ca^{2+}]. This conduction is important in the heart because it permits the rapid and organized contraction of ventricular myocytes that is necessary for the efficient generation of pressure during systole [41]. Specifically in cardiac myocytes, the initiating action potentials are propogated cell-to-cell in tissues throughout the heart, and are generated spontaneously from within pacemaker cells localized to the sinoatrial (SA) node. Cardiac action potentials are considerably slower than that which occur in skeletal muscle, with cardiac action potentials ranging from 200-400 ms in duration as compared to 2-5 ms in skeletal myocytes [41]. Non-pacemaker cells, atrial and ventricular myocytes and Purkinje cells, will serve as our example for a more detailed description of excitation-contraction coupling.

Such cells maintain a negative resting potential of around -90 mV with sarcolemmal K^+ channels open and fast Na^+ channels, as well as slow Ca^{2+} channels, closed. Action potential-triggered depolarization to -70 mV occurs rapidly through an initial opening of Na^+ channels and and continues via sustained opening of L-type Ca^{2+} channels to reach about -40 mV [41]. This Ca^{2+} influx causes further Ca^{2+} release from the sarcoplasmic reticulum (SR) [42]. This so-called Ca^{2+}-induced Ca^{2+}-release, significant in cardiac muscle, raises the cytosolic free [Ca^{2+}] ($[Ca^{2+}]_i$) from resting levels of about 50-100 nM to a peak in cardiac cells of around 1 μM [42, 43]. cTnC acts as a cytosolic buffer of $[Ca^{2+}]_i$, and the resulting increased binding of Ca^{2+} to cTnC turns on myofilaments resulting in systolic contraction. The activating depolarizations propagate cell-to-cell via gap junctions and thus throughout the entire ventricular mass, acting as functional syncytium, is activated in under 0.25 seconds [41]. Conversely, $[Ca^{2+}]_i$ levels must decline to effect the Ca^{2+} dissociation from cTnC necessary to permit relaxation and allow for diastolic filling of the heart. This is brought about by the action of the SR Ca^{2+} ATPase and sarcolemmal Na^+-Ca^{2+} exchangers, among other transporters [42].

1.2.2 Crossbridge cycle and myofilament activation

In most general terms, Ca^{2+}-dependent structural changes in Tn and altered protein-protein interactions in the affected regulatory unit alter myosin's access to actin binding by modulating the position of Tm on actin (see Figs. 7 and 8). According to the steric blocking model of Parry and Squire, Tm blocks myosin binding sites at low Ca^{2+} [44-47]. When Ca^{2+} binds to TnC, Tm shifts from the blocked position to favor the closed position that partially exposes myosin binding sites [48-50], and upon subsequent myosin bindings, Tm shifts further to the fully activated, open position. Such is the three state model in agreement with McKillop and Geeves and currently supported by structural and biochemical studies [45, 48, 51, 52]. These structural changes in the thin filament form the basis for Ca^{2+}regulation of actomyosin function when troponin and tropomyosin are present, i.e., isometric force, ATPase activity, filament sliding speed, and the kinetics of tension redevelopment (k_{TR}) [53-56].

It is important to understand the mechanics of actomyosin crossbridge cycling in order to appreciate the way in which Tn, and ultimately Tm, inhibit or enhance such interaction. Huxley's first model [57] of striated muscle crossbridge cycling describes through population dynamics the collective force generation of myosin heads by a linear elastic mechanism [57]. Experimental data has since validated a swinging lever arm hypothesis and elucidated, as well as complicated, a truer ensemble of cross-bridge models. Recognition of separation between the attachment and force-generating step has been followed by the introduction of additional mechanical and chemical states which may differ between models. Questions also exist as to whether to consider intermolecular cooperativity or explicitly treat the role of the two heads of each myosin molecule.

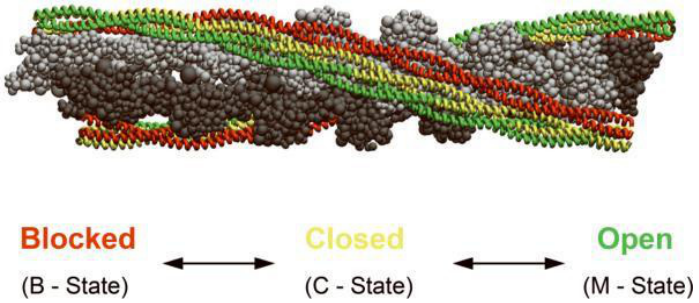

Figure 7. 3-state model of myofilament activation. The 3 average positions of Tm are depicted. In the blocked (B-) state (red), Tm resides at the outer actin domain, Ca^{2+} binding to cTnC results in an azimuthal shift to the closed (C-) state (yellow) in the actin inner domain and myosin binding drives the final shift to the open (M-) state (green). (Tardiff, 2011)

Despite ambiguity surrounding the precise order of chemical states, the mechanical powerstroke comprising the conformational changes in the myosin lever relative to actin has been evidenced by an array of structural work [58-60]. The following provides an outline of steps of the basic crossbridge cycle as recently reviewed by Bloemink and Geeves [10]. Step 1 begins with ATP binding to myosin and closure of the nucleotide pocket. This causes the 50kD cleft to open and dissociates the head from actin. Step 2: Rotation of the converter/light chain-binding domain reprimes the motor and ATP is hydrolyzed to form a stable M.ADP.P_i complex. Step 3: The lower and then upper 50kD part of the cleft rebind actin as the cleft closes. P_i is released generating tension in the form of converter domain distortion. (This event sequence is under debate.) Step 4: "Sliding": with great enough force, the load may be moved by the working stroke, dissipating the strain in the converter domain. Step 5: Nucleotide pocket opens. Step 6: ADP is released. For efficient sliding, as required of muscle myosin II, ADP release should be limited until after completion of the working stroke [10]. To date, every studied myosin with active ATPase has these same basic steps in common.

The main step in the actomyosin crossbridge cycle controlled by Ca^{2+} during activation is the strong binding of the M·ADP·P_i species to actin, with $K_d << \mu M$ [45, 61]. Referring back to the McKillop and Geeves model, this is controlled by the fraction of time Tm spends in an "open" position. Really in this case we are interested in the *accessibility* of myosin to initially weak binding sites on actin. Due to a dynamic equilibrium position of Tm, these are available to some heads in the so-called "blocked" (B) state. In skeletal muscle, Ca^{2+}-dependent changes in Tn-Tm-actin interactions, the "rolling away" of Tm, increases actin's affinity for myosin [45, 50]. The subsequent increase in number of strongly attached crossbridges displace (or stabilize the displacement of) Tm further. The precipitating changes in Tn-Tm-actin interaction originate in large part with Ca^{2+} modulation of TnI-TnC interaction, discussed in greater detail below (Section 1.4).

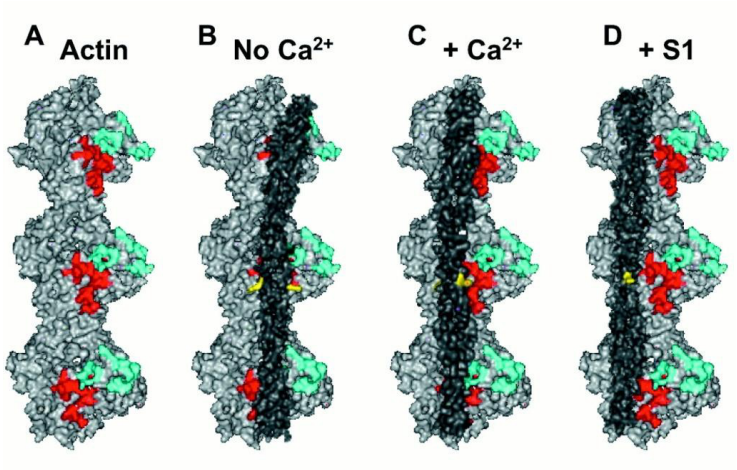

Figure 8. Tm movement over actin with varying degrees of activation. Three actin monomers of a single strand are shown in gray with light blue and red residues indicating weak electrostatic myosin interactions and stronger actin binding sites, respectively. A cardiac Tm segment in dark gray is positioned according to Xu et al., 1999. Arg90 of cTm in each strand is shown in yellow to illustrate the then-putative rolling motion of Tm. (Gordon et al., 2001)

We can intuitively see from the above how cooperativity comes into play in actomyosin binding. Cooperativity between regulatory units must also be considered. Early studies correlating pCa with isometric force in skinned muscle fibers demonstrated that Ca^{2+} activates contraction [45, 62, 63]. However, the steady-state relationship of force to [Ca^{2+}] was steeper than expected, i.e. greater than proportional to just Ca^{2+} binding [45, 64]. This prompted fitting with the Hill equation, which originally described the binding of O_2 to hemoglobin, and has since become an equation of choice in describing cooperativity among thin filament regulatory proteins [65, 66]. The Hill equation, in its nearly original form, is given by Equation 1 below:

$$y = Kx^n(1 + Kx^n)^{-1} \quad \text{(Equation 1)}$$

Applied to muscle, x would be [Ca^{2+}] and y could represent force or, in our common modification (Eqn 2), the filament sliding speed. We define pCa as -log[Ca^{2+}]. The Hill coefficient, n_H, relates specifically to the steepness of the force- (or speed-) pCa relationship around pCa_{50} and, to a first approximation, is related to the number of participating sites. For example, if single-site Ca^{2+} binding controls force with a one-to-one relation, then $n_H = 1$. Greater n_H values increase the steepness of the relationship and imply greater cooperativity of

Ca^{2+} activation. In cardiac muscle, strong crossbridge attachment also promotes Ca^{2+} binding, coupling Ca^{2+} binding with cycling crossbridge attachment and force generation as well [45, 67].

1.3 Cardiomyopathies Associated with C-TnI Mutations

Mutations in the C-terminus of TnI have been linked to a number of myopathies including Hypertrophic Cardiomyopathy (HCM) and Restrictive Cardiomyopathy, in the case of cTnI, and Distal Arthrogryposis, in the case of sTnI. Development of HCM, in particular, is influenced by a wide variety of sarcomeric gene mutations, with about 10% associated with changes in cTnI (*TNNI3*). HCM is a relatively common, yet potentially catastrophic condition, occuring in about one of every 500 individuals. Since its original description in 1958 [68] the disorder has been defined as the presence of a hypertrophied non-dialated left ventricle in the absence of any other diagnosed etiology [69] and is the most common cause of sudden cardiac death in otherwise nonsymptomatic young people.

While having some level of myocellular hypertrophy, disarray, and fibrosis in common, the range of phenotypes and clinical outcomes vary widely, as might be expected with a disorder characterized by such genetic heterogeneity. Its heritable autosomal dominance was established in 1990 [70] and this Familial Hypertrophic Cardiomyopathy (FHC) has now been linked to over 270 independent mutations in nine sarcomeric genes [69], here tabulated in Table 1 (from Tardiff, 2005.) As stated, over 25 mutations in cTnI have been implicated in FHC, at least 18 of which occur within the C-terminus. These new efforts are timely because the C-terminus of TnI is a portion of the molecule for which it has only recently been possible to develop and test detailed hypotheses about its functional role in Ca^{2+} regulation of thin filaments [31, 33, 35].

Restrictive Cardiomyopathy (RCM), in contrast to FHC, is far less common and is characterized by an incomplete filling of the ventricles while maintaining nearly normal heart wall thickness and systolic function. RCM is most often idiopathic and recent linkage studies have demostrated its relation to a point mutation in the far C-terminus of cTnI, resulting in the amino acid substitution R192H (in humans) [71, 72]. Studies employing a transgenic mouse model carrying the RCM mutation R193H (in murine cTnI) displayed phenotypes similar to human RCM patients with the analogous mutation and, functionally, showed impaired relaxation

and diastolic dysfunction [71]. Increase in the Ca^{2+} sensitivity of force production has also been demonstrated [73].

Distal Arthrogryposis (DA) is the name given to a number of skeletal muscle disorders which result in congenital limb contracture. The most common, DA type 2B, maps to chromosome 11, and is reported by Sung et al. to be caused by mutations in the C-terminus of sTnI (*TNNI2*) [74]. These mutations include a three-base in-frame deletion of a highly conserved lysine at position 167 (ΔK176del), R174Q, ΔE167del, and a truncation mutant which removes 26 C-terminal residues, R156ter [75-77]. Robinson et al showed that regulated thin filaments reconstituted with either sTnI R174Q or ΔE167del displayed greatly enhanced ATPase rates at all Ca^{2+} concentrations without change to Ca^{2+} sensitivity or cooperativity. Tn-exchanged skinned fibers with these mutants, however, showed a significant increase in Ca^{2+} sensitivity and the ΔE167del mutant, furthermore, generated significantly higher max force [76].

Table 1. Distribution of sarcomeric proteins linked to FHC

Protein	Gene	# of Confirmed Mutations	% of Total Mutations	Types
βMyHC	MYH7	116	43%	Subs >>> Trunc = Del
Reg. LC	MYL2	10	3.70%	Subs > Trunc
Ess. LC	MYL3	3	1%	Subs
cTnT	TNNT2	27	10%	Subs >>Trunc = Del
cTnI	TNNI3	24	9%	Subs >>Trunc = Del
TM	TPM1	10	3.70%	Subs
Actin	ACTC	5	2%	Subs
MyBP-C	MYBPC3	72	27%	Trunc >> Subs
Titin	TTN	1	<1%	Subs
	Total =	270		

Confirmed mutations as of June, 2005 as listed at: http://www.angis.org.au/Databases/Heart. Subs = Missense substitution, Trunc = Truncated protein, Del = Single in-frame amino acid deletion.

1.4 Function of the C-terminus of Cardiac Troponin I

Human cardiac troponin I (cTnI) (CAA62301) contains 210 amino acid residues (211 for *Mus musculus* (P48787) and *Rattus norvegicus* (AAA42294)) and possesses an additional 32 N-terminal residues not found in skeletal muscle TnI (3). Excepting this N-terminal extension, the cardiac isoforms may be thought of as broadly analogous to their skeletal counterparts, capable of being aligned about the inhibitory region (Ip) between residues 137-147 in human cTnI, residues 139-150 in mouse cTnI (2), and coinciding with residues 104-115 in rabbit skeletal TnI (rsTnI) (1). sTnI pared down to this 104-115 segment is still capable of mimicking native Ca^{2+} inhibition in skinned muscle fibers and reconstituted complexes [37]. This minimal region nearly completely inhibits actomyosin ATPase activity in the presence of Tm *in vitro* [32], hence the designation *inhibitory peptide*, an effect which is reversed by Ca^{2+}-dependent binding of the peptide to TnC when it is included within the TnI fragment of residues 1-116 [37]. These findings suggest that it may be similarly responsible for inhibition *in vivo*, while being key to switching *on* the thin filament in the presence of Ca^{2+}. Evidence that regions both N- and C-terminal to the Ip modulate ATPase activity and Ca^{2+} sensitivity stimulates reevaluation of the Ip's relative role [32, 37, 78]. Reasonably, some combination of changes in how cTnI interacts with actin, Tm, cTnT, *and* cTnC is responsible for full regulation.

A more recent characterization of TnI domains, summarized by Sykes [79], describes, adjacent to the cardiac N-terminal extension, a region tightly binding to the C-lobe of TnC (designated Rp) followed by a stretch postulated to associate with TnT. The latter is partly supported by evidence that deletion of sTnI residues 1-57 modifies interaction with TnC and wholly prevents binding of TnT [37]. As mentioned, the Sp lies C-terminal to the Ip and binds in a Ca^{2+}-dependent manner to the regulatory N-lobe of TnC. The Sp is followed in the primary sequence by at least one additional actin-binding region (Ap) adjacent to or overlapping the C-terminal mobile domain (residues 131-182 in skeletal and 164-210 in cardiac TnI) [79, 80]. It is broadly proposed that Ca^{2+} sensitivity and responsiveness of the thin filament is modulated by these C-terminal regions of TnI (most specifically, residues 96-148) [37]. This is supported by observations that binding of sTnI-(104-115) and sTnI-(96-115) increase Ca^{2+} affinity of the complex compared with sTnC alone while sTnI-(96-148) shows native Ca^{2+} sensitivity and fully

inhibits ATPase in the absence of Ca^{2+} [37]. Cardiac TnI residues 152-188 were also proven essential for Ca^{2+} sensitivity in reconstituted myofibrils [32].

H/D exchange shows that N-TnC Ca^{2+} binding altered dynamic properties (*i.e.* H/D exchange protection) near that binding site and in the TnI switch helix. (Notably, Ca^{2+} also altered dynamic properties of the Ip region that binds to actin.) These, too, support the expectation of Sp binding to the N-lobe in high Ca^{2+} [28, 36]. Using Figure 10 to illustrate, and in agreement with the "flycasting" model of Sykes [79], we might expect that as the Sp (helix 3 or H3) associates with the regulatory end of cTnC, it effectively "pulls" the C-terminal actin-Tm-binding regions away from the thin filament. That is, the dislocation of H3 is what promotes their dissociation from inhibitory attachments. It is this "tethered" relationship, proposed by Blumenschein et al., that we aimed to investigate through creation of a cTnI which incorporates a flexible hydrophobic linker between the Sp and Md. In fact, the carboxy terminus of TnI has been proposed to connect to the rest of TnI by the "flexible linker" residues 137-146 [35]. As discussed in Chapter 2, our lengthened linker could conceivably allow Sp to bind cTnC while permitting the Md to remain in an inhibitory position.

Regarding the Md function, we know loss of 23 residues is sufficient to significantly reduce cTnI inhibition in rat myofibrils and loss of ~ 40 residues causes the initial inhibition by such mutants to persist despite introduction of TnC:Ca^{2+} [32]. These roles for cTnI's C-terminus are consistent with antiparallel alignment between I and C (positioning C-TnI to bind with N-TnC). Accordingly, the the cTnI N-terminus binds C-terminal cTnC (with Ca^{2+}/Mg^{2+} sites III and IV) (Figs 9 and 10, below) [78]. As mentioned above, we know that hypertrophic cardiomyopathies have been linked to over 25 genetic mutations in cTnI and most of them are found within the C-terminal half of the protein [81]. FHC, as well as the C-TnI-associated RCM and DA type 2B mutations continue to fuel the study of these implicated domains.

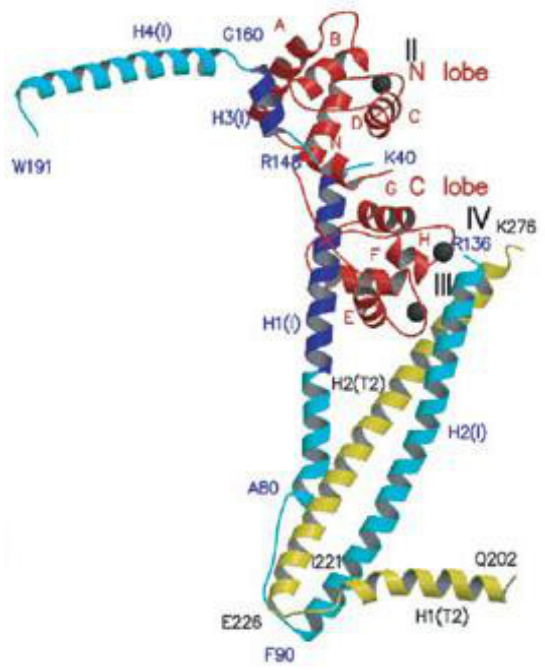

Figure 9. Ribbon diagram of 52 kD crystal structure of cTn core. cTnT (residues 183-288) is in yellow, cTnC (residues 1–161) in red, and cTnI (residues 31-210) in blue. (Takeda, et al, 2003)

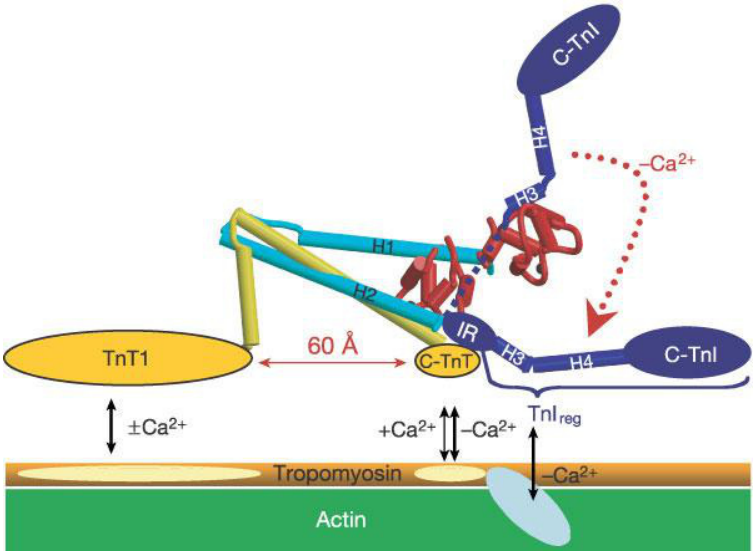

Figure 10. Proposed movement of cTnI in response to Ca^{2+}. cTnT shown in yellow, globular lobes of cTnC in red, and cTnI in blue. (Takeda, et al, 2003)

CHAPTER 2

PROBING CTNI MOBILE DOMAIN FUNCTION

2.1 Introduction: Experimental Design

Experiments were designed to consist primarily of *in vitro* motility assays that tested the functional effects of cTnI Md mutants on the sliding speed of otherwise normally regulated, reconstituted thin filaments. Filament sliding speed vs. pCa is the metric we would interpret to indicate the consequence of removal of the Md and specifically evaluate changes to the physical coupling between cTnI's Md and switch domain. We are interested in changes to pCa_{50} in particular, as well n_H and maximum and minimum sliding speeds. We know that at submaximal activation levels, kinetics are dominated by the kinetics of Ca^{2+} binding to TnC and the related transitions of the regulatory proteins. We rely in our study on the assumption that changes in activation properties (and the indices above) can be understood in terms of differences between function of the regulatory proteins [45].

Conceptually, sliding of actin filaments over HMM-treated substrate can be likened to the unloaded shortening velocity of striated muscle, and under our assay conditions, it is a reasonable analogy [82]. Like unloaded shortening velocity, thin filament sliding in IVM is similarly dependent upon cross-bridge ensembles. Ideally, it would be the effective rates of binding and release of force-generating crossbridges that determine maximum rates of filament sliding. Note that this not the same as the overall *number* of crossbridges [83]. Direction of movement is determined by the structural polarity of the actin filaments.

The optimal working concentration of regulatory proteins (cTn and Tm, being of equal ratio in all cases) to be used in experiments was selected for both mutant and wild type cTn by determining, via IVM, the minimal concentration required to affect a maximum inhibition at pCa 9, while offering consistently fast speeds at pCa 5. Note that peak motility may be reduced when [Tn + Tm] is too high [54, 84]. Typical working concentrations used with WT regulatory proteins are between 15-25 nM [84].

To test mutant effects on Ca^{2+}-dependent regulation of filament sliding (as our proxy for sarcomere contraction), IVM assays were conducted across a full range of Ca^{2+} concentrations, from that which is sufficient to arrest WT motility (1 nM) to that which enables peak WT sliding

speeds (10 μM), i.e. from pCa 9 to pCa 5. Note that 1 μM (pCa 6) corresponds to peak $[Ca^{2+}]_i$ in contracting cardiac myocytes, while 1 nM is much lower than natural resting $[Ca^{2+}]_i$. Wild type motility was generally tested at both $[Ca^{2+}]$ extremes prior to experiments to ensure comparable baselines, and at least one control assay with unregulated F-actin was conducted on each experiment day to assess variability between days and batches of proteins.

The cTnI mutants that were generated and assayed are depicted schematically in Figure 11. The first consists of a rhcTn complex containing truncated cTnI (residues 1-163) and was created by PCR-mediated insertion of a STOP codon directly upstream of K164 in its DNA sequence. This mutant construct, hereafter referred to as $cTnI_{1\text{-}163}$, removed all 46 residues of the Md, which corresponds to a mass reduction of ~5.5 kD. This was a drastic test of Md regulatory function. In line with work mentioned previously, we expected that deletions within the last 20-40 residues, and in particular this truncation, would increase Tn Ca^{2+}-sensitivity, resulting in a loss of inhibitory capability at normally inactivating Ca^{2+} levels.

The second mutant, $cTnI_{Link8}$ incorporates a flexible "linker" peptide immediately following cTnI K164 to effect a physical uncoupling of the Md from the Sp region. The linker, with a mass of ~587 D, consists of eight additional small, uncharged residues: Gly Gly Ala Val Gly Ala Gly Val. This segment was expected to have a maximum extended length of ~30 Å, calculated as 3.8 Å times number of residues, and assuming no secondary folding. We hypothesize that such an insertion will lengthen the "tether" between the Md and Sp sufficiently to permit the Sp to bind to N-cTnC in the presence of Ca^{2+} while enabling the Md to remain associated with actin. At the same time, this limited length should preclude Md binding to adjacent actin monomers. We expected that this linker insertion would likely cause loss of Ca^{2+}-

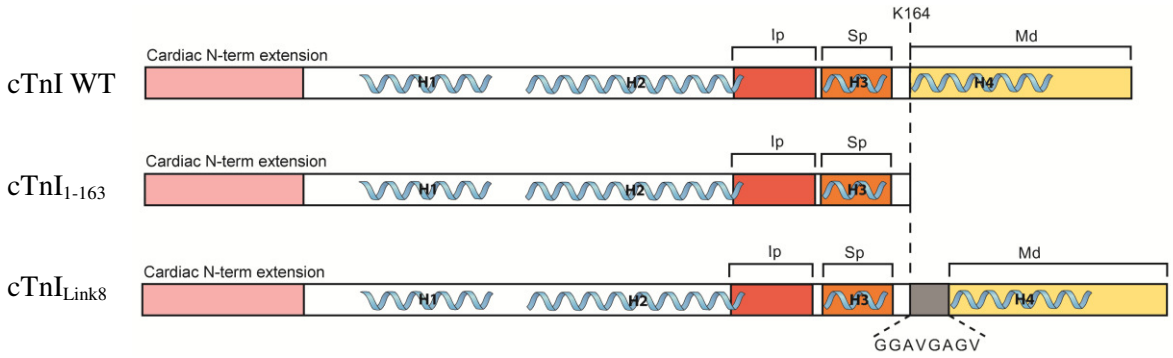

Figure 11. Schematic of cTnI sequence mutations. Mobile domain in yellow, Ip (inhibitory region) in red, Sp (switch region) in orange. Helices 1-4 as indicated. The inserted linker sequence is depicted in gray. Note the site of the truncation and insertion mutations between H3 and H4 in Fig. 10 for context.

sensitivity resulting in failure to fully activate at pCa5 (high Ca^{2+}.)

We also know that TnI's C-terminus is highly conserved across isoforms and, of the last 40 residues, 22 are charged; 15 positively, 7 negatively [37]. So alternatively, charge neutralizations (e.g. a Gly-Ala linker) adjacent to the Sp might affect the hydrophobic binding interface between TnI and TnC, and may be even more significant in cardiac TnI than in skeletal TnI in light of the proposition that binding to TnC further increases the affinity of site II for Ca^{2+} [24, 81]. It may be expected that results of C-terminal mutation within TnI might differ between cardiac and skeletal isoforms [32, 78] though these mechanistic differences are not examined here.

2.2 Materials and Methods

2.2.1 Rabbit Skeletal Muscle Preparations

Relevant protein purification procedures utilized in this work have been described in several publications [5, 53, 54, 83, 85-88]. Both the skeletal muscle myosin and actin used in the required solution biochemistry and in vitro motility studies are isolated from Adult New Zealand White rabbits (see Appendix B).

2.2.1.1 Myosin. Skeletal myosin was prepared from rabbit back muscles, an easily harvested and commonly used source for physiological studies of vertebrate contraction [88-92]. Preparations were stored in 50% glycerol at -20°C for up to six weeks. From this, heavy meromyosin (HMM) was made by mild chymotryptic digestion according to Kron et al. [91] and stored at 4°C for a maximum of three days. Prior to experiment, ATP-insensitive heads were removed by ultracentrifugation [91] and competent HMM diluted to the final working concentration (typically 250μg/ml) for use in motility assays (described below).

2.2.1.1 Actin. A fast skeletal muscle acetone powder was prepared from rabbit back and leg muscle, concomitant with myosin harvest, and stored, semi-purified, at -20°C [93]. From this acetone powder, the actin was purified according to Kron et al. [91] and stored in filamentous form (F-actin) at 4°C where it remains experimentally viable for up to one month. F-actin was labeled at least two days prior to experiment with rhodamine-phalloidin (RhPh) (Invitrogen) for visualization by fluorescence microscopy in motility assays. RhPh F-actin was diluted to 8 nM in actin buffer (AB) (25 mM KCl, 25 mM imidazole, 4 mM MgCl2, 1 mM EGTA, 1 mM

dithiothreitol (DTT), pH 7.4) [91]. Concentrations were determined spectroscopically in globular (G-actin) form prior to labeling and purity was assessed by gel electrophoresis.

2.2.2 Expression and Purification of Recombinant Human α-Tropomyosin

Human striated muscle-specific α-tropomyosin was recombinantly expressed in *E. coli* as a fusion protein with a maltose binding protein (MBP) tag for initial purification on an amylose resin-filled column (New England Biolabs, cat. # E8021S). Recombinantly expressed human regulatory proteins were used here in combination with rabbit actomyosin owing in part to availability of sufficient source material (actin and myosin) and the intention of investigating regulatory protein function as related to human disease states. Alpha-tropomyosin, specifically, is also the only isoform expressed in the myocardium of adult small mammals, and nearly so in humans [94]. All chromatography was conducted using a BioLogicLP Chromatography System (Bio-Rad, Hercules, CA, USA). Following thrombin cleavage of the MBP tag, final purification was performed via anion exchange using diethylaminoethyl cellulose resin (DE52) (Whatman, Maidstone, UK). The resulting protein (GS-α-tropomyosin) contained two extra N-terminal amino acids (Gly-Ser), which represent a conservative alternative to the AS-dipeptide in bacterially expressed Tm that substitutes functionally for N-terminal acetylation [21, 84]. Concentrations were determined spectroscopically and aliquots were stored at -80ºC until day of use. SDS-PAGE of Tm (Figure 12, lane 8) under non-reduced conditions reveals mixture of Tm monomer and dimer.

2.2.3 Coexpression and Purification of Recombinant Human Cardiac Troponin Complex

Highly purified wild-type human cardiac troponin complex (rhcTn) was recombinantly expressed in *Escherichia coli* BL21 STAR DE3 ultra-competent cells as previously reported [84]. Briefly, all three subunits cTnT, cTnI, and cTnC were coexpressed from a pET41a plasmid vector (Novagen-EMD Biosciences, San Diego, CA, USA) (see Figure 12). Two restriction sites are unique for each subunit, allowing mutagenesis to be carried out in a separate vector, and each subunit is transcribed from its own promoter. This coexpression plasmid incorporated a glutathione S-transferase (GST) affinity tag at the N-terminus of cTnT, a site that is opposite the cTnI/cTnC binding region at cTnT's C-terminus.

Initial GST-rhcTn purification from bacterial lysate was via a GST affinity column using GST-Bind Resin (Novagen-EMD Biosciences, San Diego, CA, USA), with 10 mM reduced glutathione as an elutant. The GST affinity tag removal was facilitated by a tobacco etch virus (TEV) protease site (Glu-Asn-Leu-Tyr-Phe-Gln-Gly) engineered between the GST tag and cTnT and incubation with 50 i.u. AcTEV™ protease (Invitrogen Corp., Carlsbad, CA, USA) per mg of fusion protein for 1.5 h at room temperature. Cleavage at this site results in an N-terminal extension of rhcTnT by a single amino acid, glycine. TEV protease was chosen after preliminary studies showed that several other commonly used proteases promiscuously cleaved rhcTnT [84]. GST and AcTEV™ protease were removed next in the flow-through of a DE52 (Whatman, Maidstone, UK) anion exchange column. The cardiac troponin complex, with an estimated pI of 5.15 (Scripps Protein Calculator v3.3), elutes subsequently along an increasing salt gradient. Coomassie-stained SDS-PAGE gels of purified proteins were imaged using an EDAS-290 digital imaging system (Kodak, Rochester, NY, USA) and indicate a resulting complex that is highly pure (see Figure 12 below) and functional as corroborated by motility assays demonstrating that there is no motility at pCa 9 and fast motility at pCa 5 for the WT construct at 25nM, as expected for well-regulated actin. Concentrations were determined spectroscopically using the Warburg-Christian method (DU 640 Spectrophotometer, Beckman Fullerton, CA, USA) and an extinction coefficient at A_{280} of 30110 $M^{-1}cm^{-1}$, estimated by the method of Gill and von Hippel [95]. Aliquots were stored at −80ºC until day of use.

2.2.4 Coexpression and Purification of Mutant Recombinant Human Cardiac Troponin Complex

For purposes of mutagenesis, the region containing strictly cTnI and flanking sequences from the coexpression vector (Figure 13) was excised and cloned into the smaller pCR 2.1 TOPO vector (Invitrogen). Conducting mutations in this slimmer construct served to eliminate amplification errors encountered due to the redundancy of sequences that flank each subunit. Subsequently, mutated cTnI was cloned back into the former pET41a vector using StuI and HindIII (Invitrogen) restriction enzymes and transformed into BL21 STAR *E.coli* as referred to above for expression and purification.

Specifically, $cTnI_{1-163}$ incorporates three adjacent UAA (bacterial STOP) codons immediately prior to K164 in the DNA sequence. Presumably, only a single STOP is actually necessary. The mutation was engineered by site-directed PCR mutagenesis (PCR-SDM) of WT

cTnI in the TOPO vector. The $cTnI_{Link8}$ contains eight additional residues (Gly Gly Ala Val Gly Ala Gly Val) just C-terminal to WT K164. This adds a mass of ~587 D. The corresponding DNA codon sequence, 5' GGT GGT GCA GTT GGN GCA GGT GTT 3', was introduced into WT cTnI via three sequential rounds of PCR-SDM, also in a TOPO vector.

The purification strategy described for WT rhcTn was also employed for mutants because there were minimal charge alterations resulting from incorporation of the cTnI mutants into the coexpression vector (in place of WT cTnI) due, in part, to the complex's high net charge. Changes to pI were estimated at less than 0.1 unit. As the linker contained no Trp, Tyr, or Cys residues, no change to the extinction coefficient used to quantify the $cTnI_{Link8}$ complex was deemed necessary. For the complex containing $cTnI_{1\text{-}163}$, we used an extinction coefficient at A_{280} of 24420 $M^{-1}cm^{-1}$ calculated with Scripps Protein Calculator v3.3 [95].

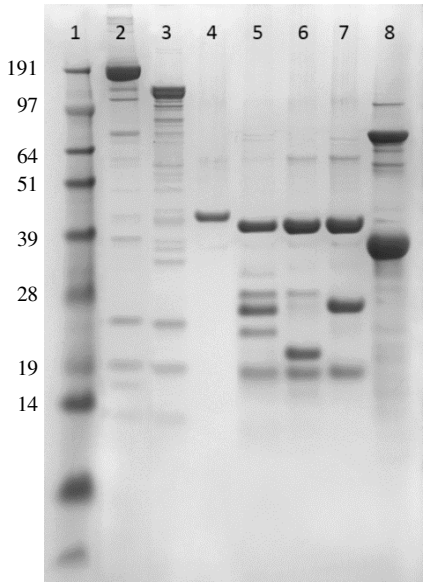

Figure 12. SDS-PAGE gel of purified proteins.
Lane 1, MW marker (Invitrogen)
Lane 2, rabbit skeletal myosin
Lane 3, rabbit skeletal HMM
Lane 4, rabbit skeletal actin
Lane 5, rhcTn WT
Lane 6, rhcTn with cTnI K164STOP
Lane 7, rhcTn with cTnI K164Linker
Lane 8, human recombinant α-tropomyosin

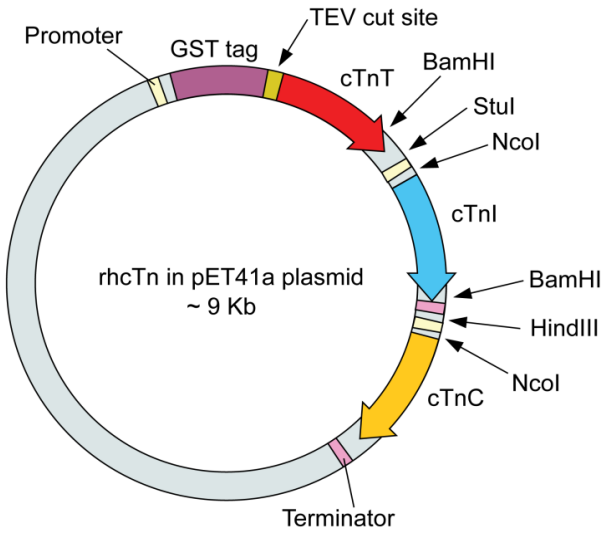

Figure 13. Schematic of modified pET41a coexpression vector. Showing placement of subunit and GST tag sequences.

2.2.5 *In Vitro* Motility Assays

In vitro motility assays with regulated actin were carried out using the general methods described previously [5, 83, 85, 96]. Flow cells were formed on cleaned glass slides from nitrocellulose-coated cover slips and glass spacers, held together by vacuum grease [5, 53, 54, 83, 85-88, 96, 97].

2.2.5.1 Solutions. Solution aliquots were equilibrated to room temperature (in the pipette tip) to degas (and avoid bubble formation that can denature proteins) within the flow cell. Infused solutions (>2X chamber volume) were left for 1 minute (or longer, as noted below) in the flow cell chamber and then flushed with AB before infusing the next solution. HMM was applied first, allowing initial adsorption onto the nitrocellulose-coated substrate, followed 1 minute later by 0.5 mg ml^{-1} bovine serum albumin (BSA) in AB, which acts as a blocking agent to passivate any remaining exposed nitrocellulose surfaces.

After the chamber is flushed with AB, unlabeled F-actin (~100 μg ml^{-1}, sheared by at least 15 rapid passages through a 23-gauge needle) is added, followed 1 minute later by a flush with AB solution. Then AB with 0.5 mM ATP is added to dissociate the remaining unlabeled F-actin from competent HMM, thus leaving residual "dead heads" blocked by unlabeled F-actin [48, 98]. After another flush of the chamber with AB, RhPh F-actin is applied in the absence of ATP. Labeled actin filaments that do not bind to HMM on the surface are flushed from the chamber with a wash buffer (WB) consisting of either AB for assays with unregulated RhPh F-actin, or AB plus Tn and Tm (typically~25 nM each) for assays involving regulated thin filaments. Reconstituted RhPh F-actin filaments with AB plus Tn and Tm are incubated in the flow cell chamber for three minutes to allow for assembly of regulatory complexes, followed by final infusion of the ATP-containing motility buffer (MB) to initiate filament sliding resulting from actomyosin ATPase activity.

Control assays with unregulated RhPh F-actin were conducted in AB [48] with 2 mM ATP and 0.3% methylcellulose (MC), or at pCa 5 and 9 (details below) without added cTn and Tm. Standard solution composition for assays with regulated RhPh-labeled thin filaments was: 2 mM MgATP, 1 mM Mg^{2+}, 10 mM EGTA, sufficient calcium acetate to achieve the desired pCa between 9 and 4 (pCa = - log [Ca^{2+}], where [Ca^{2+}] is in molar), 50 mM K^+, 15 mM Na^+, 20 mM MOPS, pH 7.0 at 30°C, 0.3% MC, and troponin and tropomyosin (typically ~ 25 nM each). Ionic strength was adjusted to 0.085 M with TrisOH and acetic acid. All motility buffers also

contained 3 mg/ml glucose, 100 μg/ml glucose oxidase, 18 μg/ml catalase, and 40 mM DTT which was found to be necessary to minimize photobleaching of the fluorophores and photo-oxidative damage to the proteins for the duration of observation. Individual fields were illuminated for a duration of ~30-60 seconds each. Total imaging time for a given flow cell averaged roughly 5-10 minutes.

2.2.5.2 Microscopy and acquisition. Following final infusion of MB into the flow cell, the slides were transferred to the stage of a Nikon Eclipse TE2000-U inverted fluorescence microscope (Nikon Corporation, Tokyo, Japan) with both Hg and TIRF (green HeNe and blue argon lasers) illumination. An empirically optimized standard steady state temperature of ~30°C within flow cells was maintained by an objective heater coil (heater model no. OH30 and B600 temperature controller, 20/20 Technology, Inc, Wilmington, NC, USA).

RhPh-labeled filaments were imaged with a SIT camera (Model VE1000; Dage-MTI, Michigan City, IN) and video was recorded onto DVD at 30 frames per second with an added time-date generator signal (Model WJ-810, Panasonic, Secaucus, NJ). Typically, six fields were recorded for >30 seconds each for every flow cell (i.e. each experimental condition).

2.2.5.3 Data analysis. Our lab had previously used custom Linux-based software utilizing C++-coded image analysis with scripting and interface modules written in Python. This was analogous to our previously described method [5, 53, 54, 85, 88, 97], following that of Homsher and Sellers [99, 100]. The software read as input a series of images and outputs a list of filament tracks, listing every filament edge's center of mass, length, head and tail for all of its constituent frames. User-defined parameters controlled variables like edge-thresholding and minimum track length, and a filament's path and speed statistics calculated only when that centroid could be unambiguously tracked for at least 2 s. We had found that this automated method of analysis, however, did not adequately characterize filament length or average speed for short time intervals and so a more manual approach was taken.

The primary method for quantifying filament sliding speed and filament length was thus through ImageJ 1.41 software (available at http://rsb.info.nih.gov/ij; developed by Wayne Rasband, National Institutes of Health, Bethesda, MD). First, DVDs were ripped to hard drive storage using AOA DVD Ripper 5.1.9 (Copyright © 2008 AOAMedia) and the digital tracks containing the recorded data for each of the fields were converted into a stack of 90 frames using VirtualDub 1.8.6 freeware (Copyright © 1998-2008 Avery Lee).

This generally yielded a sampling of every tenth frame. Stacks were imported into ImageJ and image contrast was enhanced by subtracting background using a "rolling ball" algorithm to remove smooth continuous background [101]. For each stack, approximately ten to twenty filaments were randomly selected and, in ImageJ, the distance traveled by a given filament and its length were determined. Manual tracking of its leading edge was performed using the ImageJ plugin MTrackJ in a frame-by frame fashion for the duration of its movement or presence within the frame boundaries. Figure 14 shows examples of MTrackJ tracking of filaments at both pCa 5 and pCa 9. Each color indicates a separate filament trajectory. Filaments not tracked in Figure 14b displayed no discernible translocation. Average speed (in μm/s) was obtained by dividing the distance traveled (in μm) by the duration of its tracking.

The ratio of standard deviation/mean speed was calculated for each path as an indicator of motion uniformity [54, 99, 100]. A filament was accepted as moving uniformly when this ratio was < 0.3. The fraction of filaments moving uniformly in each flow cell (one condition), and the unweighted mean speed (± SD) of those filaments was obtained by combining information from all filament paths recorded. Analyses combined all speeds from replicate flow cells at different pCa values. A modified form of the Hill equation (Eqn 2) was fit to speed-pCa data for regulated F-actin using nonlinear least squares regression analysis (SigmaPlot Version 11, Systat Software, Inc., Chicago, IL, USA).

$$s = s_{max}\,(1+10^{n\,(\,\mathrm{pCa}-\mathrm{pCa}_{50})})^{-1} + s_{min} \qquad \text{(Equation 2)}$$

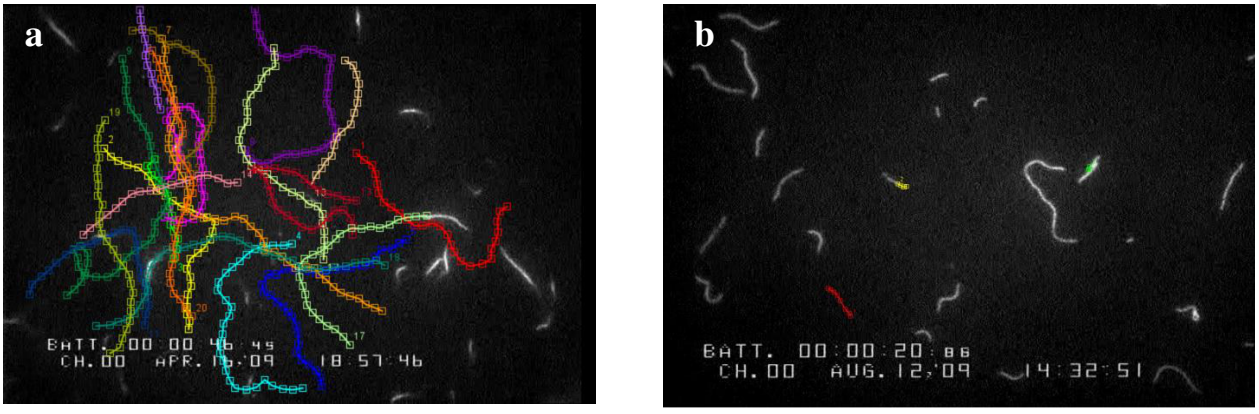

Figure 14. Filament tracking in ImageJ using MTrackJ. (a) Representative example of regulated filaments at pCa 5, and (b) at pCa 9, tracked over 30 s total.

Regression parameter s_{min} represents the speed obtained at low [Ca^{2+}] (here, pCa 9), and s_{max} is the Ca^{2+}-activatible increment in speed. Speed at saturating Ca^{2+} (here, pCa 5) equals s_{max} plus s_{min}. pCa_{50} is equal to the pCa at the midpoint of the Ca^{2+}-dependent portion of the speed-pCa relationship (i.e., for $s = (s_{max}/2) + s_{min}$) and n_H describes the cooperativity as reflected in the steepness of the relationship plot around pCa_{50}. The data were normalized to ($s_{max} + s_{min}$) to allow comparisons between data collected with the two different batches of myosin used in this study. Unless otherwise specified, regression errors are standard errors for the regression parameters.

2.3 Results

2.3.2 Working Concentrations

The Tn/Tm concentration at which assays were conducted was chosen based on evidence of that which elicited a maximum sliding speed at pCa 5 while maintaining the minimum speed at pCa 9. The WT cTn was thus assayed at 25 nM, which fit the criteria above as displayed in Figure 15a, and is commonly used in regulated IVM experiments. Assays incorporating the $cTnI_{Link8}$ mutant met these same criteria best at 50 nM. While the $cTnI_{1\text{-}163}$ mutant came least close to these criteria at any concentration, this ambiguity directed us to using it at 50 nM as well, primarily for the sake of comparability (see Fig. 15).

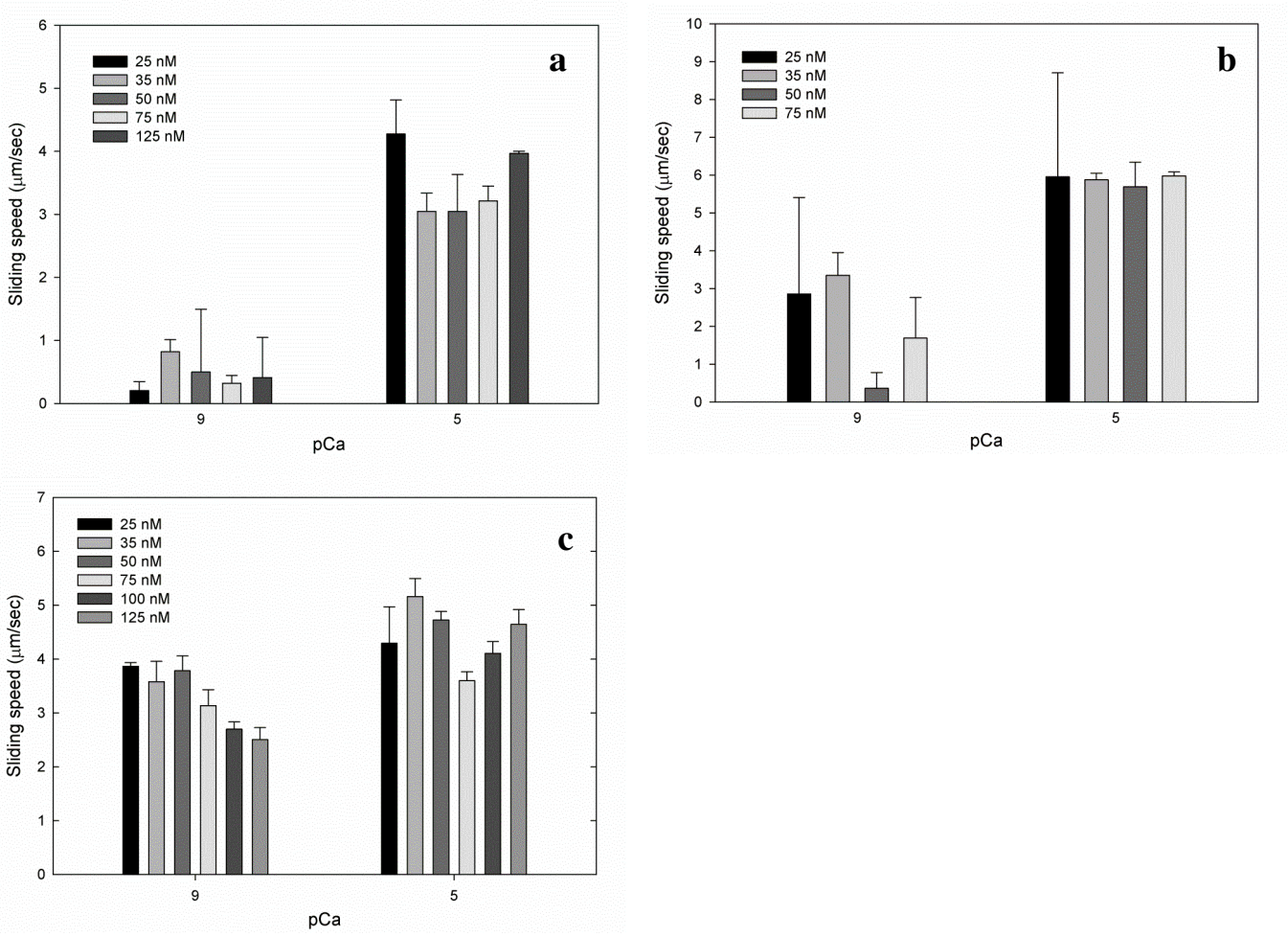

Figure 15. Effect of regulatory protein (Tm/Tn complex) concentration on filament sliding speed. Incorporating (a) WT cTn complex, (b) $cTnI_{Link8}$ complex, or (c) $cTnI_{1\text{-}163}$ complex.

2.3.2 Speed-pCa Relationships

2.3.2.1 Wild-type cardiac troponin complex. As seen in Figure 16a**,** maximum sliding velocity ($s_{max} + s_{min}$, Eqn 1) was 10.9 ± 0.7 μm s^{-1} as compared to 9.2 ± 1.0 μm s^{-1} for unregulated filaments in the same experiment (data not shown). Speed values were normalized to this average unregulated speed (Fig. 16b), indicating a 1.2-fold increase in the maximum speed when WT cTn and Tm (25nM) are present with saturating Ca^{2+}. Minimum sliding velocity (s_{min}) achieved here at pCa 9 was effectively zero: the majority of filaments showed no discernable translocation or exhibited higher-than-threshhold erraticity. The pCa_{50} value was typical of regulated filaments at 5.98 ± 0.02 and the Hill coefficient, n_H, was estimated at 6.8 ± 2.7, indicating significant cooperativity. Figure 17 shows normalized data from a later repeated experiment performed with labmate Linda Stroud which suggests a similar pCa_{50} value and surrounding slope (n_H). (Detailed data from this last experiment is not currently available to me and its plot is shown as corroborative with limitations.)

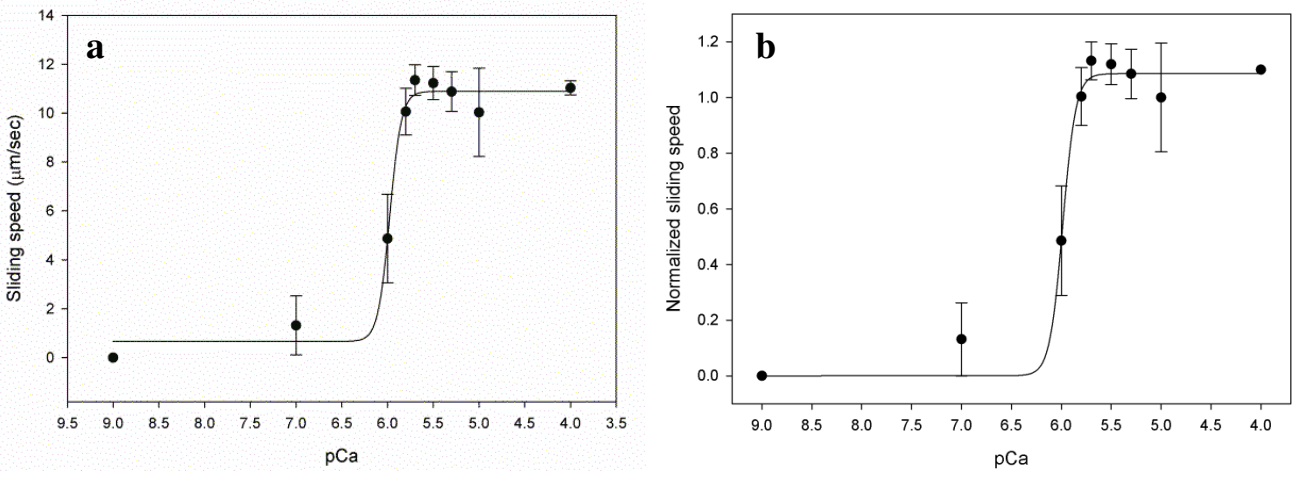

Figure 16 (above). Ca^{2+}-sensitivity of sliding speed with WT cTnI, 25nM. (a) Raw data, (b) normalized to ($s_{min} + s_{max}$). Error bars indicate standard deviation.

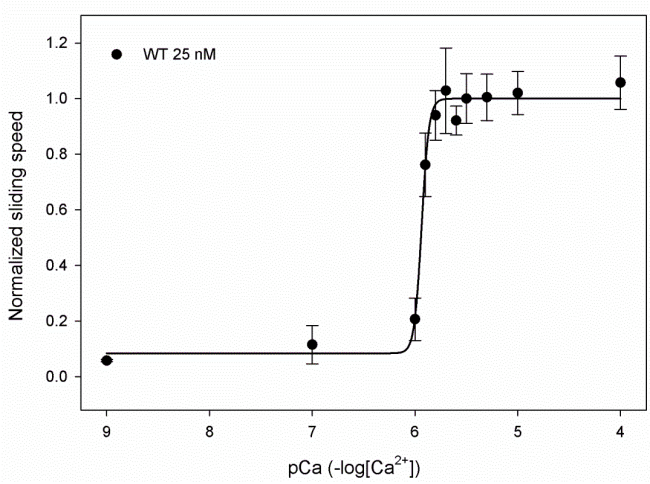

Figure 17 (left). Ca^{2+}-sensitivity of sliding speed with WT cTnI, 25nM, with Linda Stroud. Data normalized to (s_{min} + s_{max}). Error bars indicate standard deviation.

2.3.2.2 $cTnI_{1\text{-}163}$ complex. Experiments with each mutant were conducted twice, on separate days using distinct batches of myosin as the HMM source, i.e. $cTnI_{Link8}$ Trial 1 and $cTnI_{1\text{-}163}$ Trial 1 shared the same myosin source (i.e. preparative batch), and similarly, each Trial 2 at a later date. Within trials, filaments regulated with $cTnI_{1\text{-}163}$ displayed maximum sliding speeds comparable to those of WT cTn-regulated filaments. Modeling of the Trial 1 raw data gives a maximum and minimum speed of 5.6 ± 0.5 and 4.7 ± 0.3 μm s^{-1}, respectively. Trial 2 resulted in relatively higher values, but also showed decreased inhibition at pCa 9, with raw values of 14.8 ± 0.6 and 9.0 ± 0.4 μm s^{-1} for maximum and minimum velocity. Minimum sliding speeds achieved at pCa 9 were higher than with WT cTn, with $cTnI_{1\text{-}163}$ filaments displaying an inability to achieve full inhibition at low Ca^{2+} (Fig. 18). Normalized sliding speed at pCa 9 was ~79% of the maximum (set to 1.0 in all cases) in Trial 1 and ~61% of the maximum in Trial 2. Apparent in all $cTnI_{1\text{-}163}$ assays was a dramatic increase in Ca^{2+} sensitivity indicated by an increase in pCa_{50} from ~5.99 for WT to > 6.5 (the $cTnI_{1\text{-}163}$ pCa_{50} values were not determinable from the data). See Table 2 for parameter values. Note the poor fit to data in the $cTnI_{1\text{-}163}$ Trial 1, which, with this mutant, justifies not combining data from Trials 1 and 2.

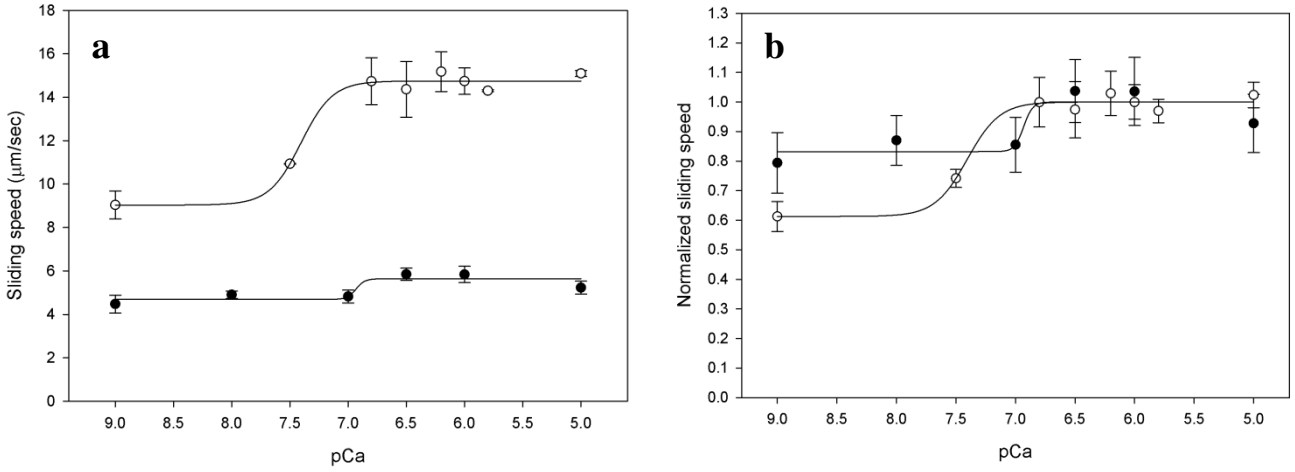

Figure 18. Ca^{2+} sensitivity of sliding speed with $cTnI_{1-163}$, 50 nM. (a) Raw data, (b) normalized to (s_{min} + s_{max}) of the given data set. Filled circles (●) represent data from Trial 1, open circles (○), data from Trial 2. Error bars indicate standard deviation.

It is perhaps important to account for the difference in maximum velocities between the two trials and this will be addressed in Chapter 3. In part because of these differences, the poor fitting in $cTnI_{1-163}$ Trial 1, and despite the normalization to each set's own (s_{min} + s_{max}) as described in 2.2.5.3, the fits to the data of different trials will be plotted independently.

2.3.2.3 $cTnI_{Link8}$ complex. Filaments activated fully at pCa 5 and neither maximum nor minumum normalized sliding speeds were greatly affected by incorporation of the $cTnI_{Link8}$ mutant. Modeling of the Trial 1 raw data gives a maximum and minimum velocity of 4.1 ± 1.3 and 1.1 ± 0.9 µm s^{-1}, respectively. Trial 2 gave 14.6 ± 1.5 and 0.4 ± 1.01 µm s^{-1} for raw maximum and minimum speeds. Similarity to those of WT cTn-regulated filaments is reflected in a comparison of s_{max} and s_{min} fits to normalized data, seen in Table 2. As in 2.3.2.2, data from each trial is plotted independently.

Incorporation of the 8-residue linker did also result in a substantial increase in Ca^{2+} sensitivity (ave pCa_{50} shift of 0.97 units, or 6.95 as compared to 5.98 for WT cTn) (Fig. 19). Normalized sliding speed at pCa 9 was ~26% of the maximum in Trial 1 and ~1% of the maximum in Trial 2.

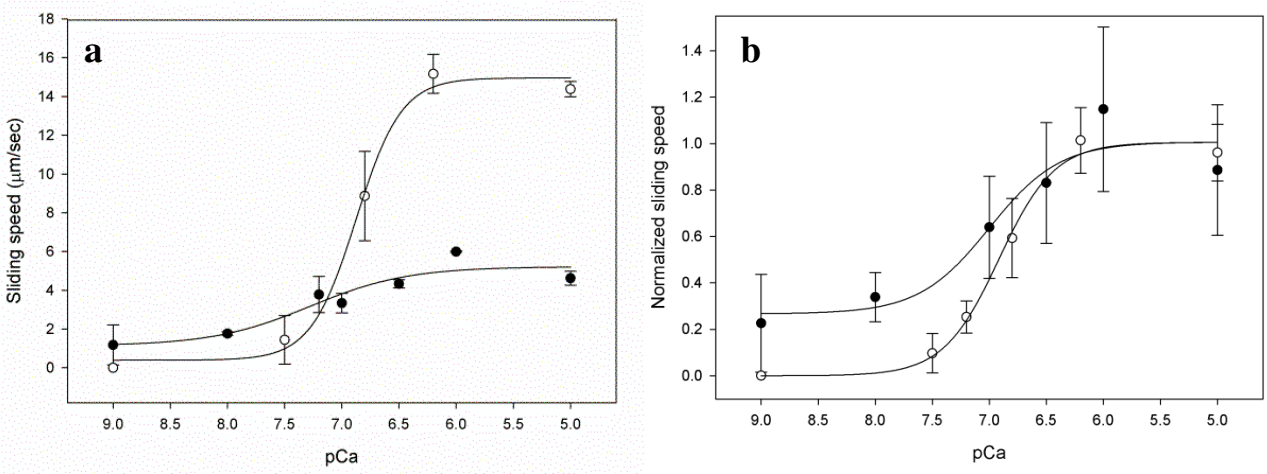

Figure 19. Ca^{2+} sensitivity of sliding speed with $cTnI_{Link8}$ mutant, 50 nM. (a) Raw data, (b) normalized to (s_{min} + s_{max}) of the given data set. Filled circles (●) represent data from Trial 1, open circles (○), data from Trial 2. Error bars indicate standard deviation.

Figure 20 provides a comparison between the WT, $cTnI_{1\text{-}163}$ and $cTnI_{Link8}$ complex speed-pCa curves. As the plot contains just Trial 2 data for the mutants, it represents assay results from a single, shared myosin preparation. Notice that of maximum and minimum velocities, only the minimum velocity of the $cTnI_{1\text{-}163}$ complex is much altered. Differences in pCa_{50} are apparent, as are the differences between each mutant and WT n_H values. Regarding these Trial 2 fitted n_H values, the $cTnI_{Link8}$ data as it has an associated confidence interval (95%) of 0.00 - 3.67. That of the $cTnI_{1\text{-}163}$ data is 0.00 - 6.42. Thus while we draw little conclusion regarding the change in n_H seen between WT and $cTnI_{1\text{-}163}$ data, we conclude a decrease in cooperativity between WT and $cTnI_{Link8}$ data as evidenced by the change in n_H of 4.8 units, from 6.6 to 1.8 (Trials 2 in Table 2).

Table 2. Fits of Equation 2 to normalized IVM data.

Parameter	WT Trial 2	$cTnI_{1-163}$ Trial 1	$cTnI_{1-163}$ Trial 2	$cTnI_{Link8}$ Trial 1	$cTnI_{Link8}$ Trial 2
R^2	0.98	0.78	0.99	0.93	0.99
n_H	6.63	11.50 *	3.19	1.35	1.78
pCa_{50}	5.99	6.93 *	7.41	6.99	6.92
smin	0.00	0.83	0.61	0.28	0.00
smax	1.00	0.17	0.39	0.80	1.00

Asterisks indicate failure of the model to converge and therefore these values, and data in this trial generally are less reliable than the others. For WT and $cTnI_{Link8}$ Trial 2 fits, s_{min} was constrained to zero.

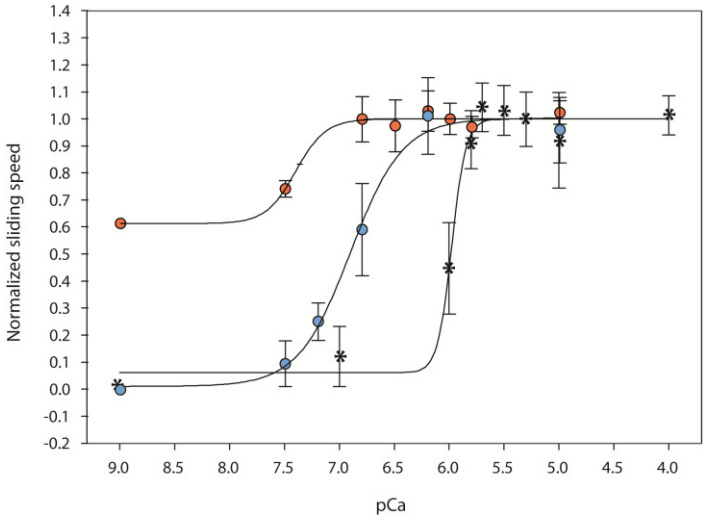

Figure 20. Superimposition of Trial 2 speed data. WT (∗), $cTnI_{1-163}$ (peach), and $cTnI_{Link8}$ (cyan) shown. Data normalized to unregulated filament velocity with s_{max} scaled to 1.0 (as in Figs 16c, 18c, and 19c). In this figure, s_{min} is not contrained to zero, as is in Figures 16b and 19b (Trial 2). Error bars indicate standard deviation.

CHAPTER 3

CONCLUSIONS AND FUTURE WORK

Our results indicate that the Md is essential for full inhibition of Ca^{2+}-regulated filament sliding in the *in vitro* motility assay. This was not unexpected, as a removal of the Md is unlikely to represent a neutral mutation based on the earlier work of Rarick and others [32, 37, 102]. Our removal of the Md also caused a marked increase in Ca^{2+} sensitivity. As mentioned, FHC-associated mutants in cTnI are most prevalent within the C-terminus and its noteworthy that of these fifteen or so mutations, a majority have exhibited the effect of increasing Ca^{2+}-sensitivity [69]. C-terminal truncation of sTnI (Δ156ter), too, displayed increased Ca^{2+}-sensitivity in skinned fiber DA models. (Recall that increased Ca^{2+}-sensitivity also resulted from the C-terminal cTnI RCM mutant, R173H.) Thus, it was expected that such would be the effect of removing the Md from cTnI, inasmuch as presumably we would see a loss of the complex's ability to inhibit filament motility at low [Ca^{2+}]. That is, we would see filaments requiring lower concentrations of Ca^{2+} to activate as compared to those regulated by WT cTn. The IVM results with $cTnI_{1\text{-}163}$ reported above supported this expectation with an apparent increase in pCa_{50} of at least 0.5 units.

We found that removal of the Md had little or no effect on IVM maximum (Ca^{2+}-saturated) filament speed. That removal of the Md had no effect on this parameter is consistent with the fact that regulatory proteins have been found to have little to no effect on actomyosin S1 ATPase V_{max} in solution when Ca^{2+} is bound to Tn [103].

Regarding incorportion of the $cTnI_{Link8}$ mutant, we had hypothesized that a consequence of incorporating the 8-residue flexible linker would be that it effectively decouples the expected "push and pull" between the Md and Sp. Were this the case, we expected the complex to fail to "turn on" at activating levels of Ca^{2+}. This predicted *loss* of Ca^{2+}-sensitivity could result, hypothetically, from the ability of the Sp domain to bind appropriately to the N-terminus of cTnC in response to Ca^{2+} while the flexible linker still permitting the actin-binding region of the Md to remain attached to actin-Tm (its proposed inhibitory position). Change in Ca^{2+}-sensitivity with this mutant could also conceivably result from an unforseen interaction of the hydrophobic linker with the N-terminus of cTnC, though this possibility was not to be pursued within the

scope of this project. My preliminary results, however, indicated an *increase* in Ca^{2+}-sensitivity, which begged reconsideration of a more dynamic equilibrium between the "on/off" positions of Ip-Sp-Md, in which a more permissive range of motion enabled by the insertion may *favor* Sp binding to N-cTnC (a speculation).

Following further analysis we found that disrupting the sequential connection between the Md and Sp by insertion of the flexible 8-residue linker did NOT inhibit Ca^{2+}-dependent activation of the thin filament (contrary to hypothesis). This insertion resulted in relative maximum/minimum filament speeds similar to that seen with the wild type. We did find that the insertion, like $cTnI_{1\text{-}163}$, resulted in an increasing shift in Ca^{2+} sensitivity, though slightly less than that of $cTnI_{1\text{-}163}$, and that it decreased cooperativity.

It is important to address the variation in range of speeds seen between Trial 1 and Trial 2 assays. Unregulated filament sliding speeds were nearly 2-fold higher in Trial 2 assays than in Trial 1. A first assumption is that the lower speeds of Trial 1 must be "correct" as they are more in line with our lab's previous IVM work and that of others [45, 84, 104], however an explanation for the difference is lacking. My prospectus proposed measuring both K^+-EDTA and Ca^{2+}-ATPase activities for each myosin preparation [92]. This was not done, but could have provided clues as to the speed discrepancy. Kinetic variations exist between myosins prepared from different muscle types. See for example, Bloemink and Geeves, 2011 and Schoffstall et al, 2006. It is of some assurance that Schoffstall et al. found that regulated thin filament function is uneffected by actomyosin kinetics [84]. However, sliding speed variations between isoforms can be significant and, in our case, may have resulted from inadvertent differences in muscle type harvested. It has been shown that *in vitro* filament sliding velocity correlates strongly with HMM-ATPase rate [105]. The as-yet unexplained baseline speed difference between Trial 1 and 2 and the poor fit of the model to the data in the $cTnI_{1\text{-}163}$ Trial 1 are reasons why data from the two trials were not pooled here. In addition, WT data from the myosin preparation of Trial 1 was not collected, therefore a precluding a proper comparison.

Regarding follow-up studies, it was planned that if no effect was seen with $K164_{Link8}$, the length of the insert would have been doubled to at least16 residues, a $\geq$ 2X repeat of the initial sequence, to facilitate greater separation of the Sp and Md. A possible complication of such an increase is that the longer tether might enable the Md to associate with an adjacent actin monomer. Alternatively, charge neutralizations (e.g. a Gly-Ala linker) within this region could

have *decreased* Ca^{2+} sensitivity owing to impaired TnC:TnI interactions (or maybe increased affinity for actin-Tm.) Another avenue of investigation could have been the insertion of the original linker construct between the Ip and Sp near residue I149, as a comparison between the inhibitory contribution of the Ip versus the Md's adjacency to the switch region. This could have begun to examine whether Sp binding to N-cTnC is critical to "pulling" Ip toward its inhibitory binding position on cTnC [79]. Having gotten the necessary molecular biology routines firmly in place, it was reasonable to envision several possible mutational variations to this region of cTnI to be planned as the initial results may have dictated.

Original plans of adding the C-terminal peptide, $cTnI_{165-210}$, alone to thin filaments lacking the remainder of the complex was expected to result in a loss of perhaps all Ca^{2+}-sensitivity**,** which could conceivably be caused by binding of the fragment to actin autonomously. This clearly would represent an absolute decoupling; an "infinite length" linker, so to speak. The extent to which Ca^{2+}-independent *in vitro* motility would be attenuated in the presence of this peptide could depend upon its independent affinity for its actin binding site. Binding may be weak enough without support from the intact complex and, specifically, the connection to an actin-bound Ip, that little effect would be observed. Conversely, binding could be of sufficient affinity and/or promiscuity in its location of binding that motility is prevented. The latter could include the binding of one Md peptide per actin monomer as opposed to one per regulatory unit when part of intact Tn, or its association with other unpredicted sites. Such possibilities would have been investigated by pairings of the peptide with both WT and the mutant cTnI complexes in regulated IVM assays.

An expression plasmid was constructed utilizing our modified pET41a construct that included a GST affinity tag preceding the sequence coding for peptide $cTnI_{165-210}$. A TEV protease cut site was included between these two to facilitate GST tag removal, as in the rhcTn purification, purification would likely involve an initial GST affinity column followed by tag cleavage and subsequent HPLC size-exclusion chromatography. While this particular effort was eliminated from the scope of this thesis, it would likely be on the top of the list of things to revisit upon a furtherance of these experiments.

APPENDIX A

SnO_2 NANOBELT FIELD-EFFECT TRANSISTOR DETECTION OF CARDIAC TNI

Cardiac troponin I has long been used as an important clinical indicator of myocardial injury. Upon trauma to the heart, damaged myocytes may release indicative proteins into the bloodstream and the tracking and analysis of these various markers has greatly contributed to an understanding of the pathophysiology of a spectrum of coronary syndromes and, significantly to the clinician, to the stratification of patient cardiac risk (12).

In the last decade, the cardiac troponin subunits T and I have gained preference as indicators of myocardial damage in part due to their relative specificity to *cardiac* injury; both cTnI and cTnT represent cardiac-specific isoforms (co-released TnC is shared among muscle types and its levels thus less diagnostically conclusive.) cTnI and cTnT, while in a sense structural, also exist in cytosolic pools within myocytes and display both early and sustained concentration levels post-trauma in the bloodstream (12) and these can be critical in rapidly assessing and monitoring a patient's status. Other characteristics such as molecular size, which may influence release and clearance rates, solubility, stability, and detectability factor into these markers' utility and the design of detection assays.

Sandwich ELISA is still currently the primary method used to quantitate biomarker levels in patient blood, in particular cTnI, and laboratory tests are commonly performed conventionally in microtiter plates. These assays can inform the choice of treatment following a cardiac emergency and are being developed into hand-held, point-of-care (POC) assay devices utilizing miniscule blood or plasma samples. They function much like drugstore pregnancy tests, indicating results within about 20 minutes. While this represents an improvement, it remains of keen interest to improve the speed, reliability, reusability, and accuracy of devices to detect the presence of cTnI or its proteolytic fragments.

In this context, Yi Cheng and coworkers in the Florida State University Department of Physics and Integrative NanoScience Institute began developing field-effect transistor (FET) sensors for label-free detection of cTnI. These transistors are three-terminal semiconductor devices: one terminal controls electrical resistance or current flow between the other two terminals, giving transistors a valvelike operation. Importantly, they can amplify signals over

some linear range of voltage and current. The device integrated a microfluidic channel to permit flow of analyte past an active functionalized SnO_2 nanobelt, upon which association of analyte to the nanobelt would alter its electical conductance and signal binding and relative concentration.

Validation of the sensing scheme was first demonstrated by detection of biotin-streptavidin binding, i.e., devices with single biotinylated SnO_2 nanobelts showed pronounced conductance changes in response to streptavidin binding. Yi Cheng demonstrated that the pH-dependence of the conductance changes was fully consistent with the predicted protonation states of streptavidin, and Figure A2c shows how specificity of the sensors' electrical responses was confirmed by fluorescence imaging from streptavidin-coated quantum dots. The devices were then functionalized with biotinylated anti-cTnI monoclonal antibodies (mAb). They exhibited high sensitivity to that antigen, while showing no measurable responses to control proteins such as BSA and cardiac Tm. The study demonstrated the potential of the nanobelt FET as portable sensors for rapid, on-site detection of biomedically significant markers.

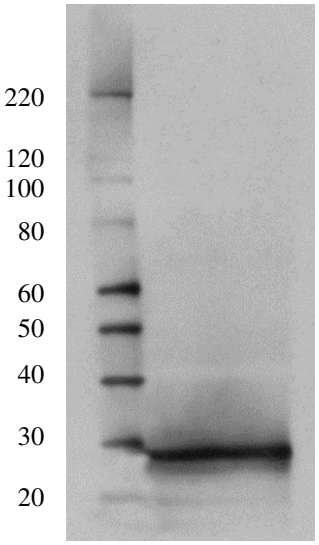

Figure A1. Detection of cTnI by primary mAb clone 16A11.
NuPAGE 4-12% Bis-Tris, MOPS. MagicMark ladder.

Recombinant human cardiac troponin complex was prepared as described and tested for recognition by several monoclonal antibodies (mAb) against human cardiac troponin I. Reliable recognition was achieved with an IgG_1 mouse mAb, clone 16A11 (Cat. No. 10R-T123f, Fitzgerald Industries International, Inc., Concord, MA, USA.) at a stock dilution of 1:50,000,

using as a secondary antibody polyclonal goat anti-mouse HRP conjugate (BioRad Cat. No**.** 170-5047) at a 1:60,000 dilution. See Figure A1. Chemiluminescent detection employed Immun-Star™ HRP substrate products (luminol enhancer and peroxide buffer, BioRad Cat. No. 170-5040.)

The mAb 16A11 was biotinylated using Sigma-Aldrich Immunoprobe™ Biotinylation Kit (Cat. No. BK-101) with an average of 3.2 biotin molecules per IgG molecule, as determined by HABA assay (reagents provided in Immunoprobe™ kit.) There was little or no effect of biotinylation on antibody function, as assessed by Western blotting (image not shown). Recombinant streptavidin (*Streptomyces avidinii*) was provided from Roche (Cat. No. 11 721 666 001.) Recombinant human cTnC, α-Tm, and BSA were provided as controls for detection specificity. Advice was additionally provided to Yi regarding the permissible pH ranges for testing the device, protein stability, protein-protein affinities, and buffer considerations.

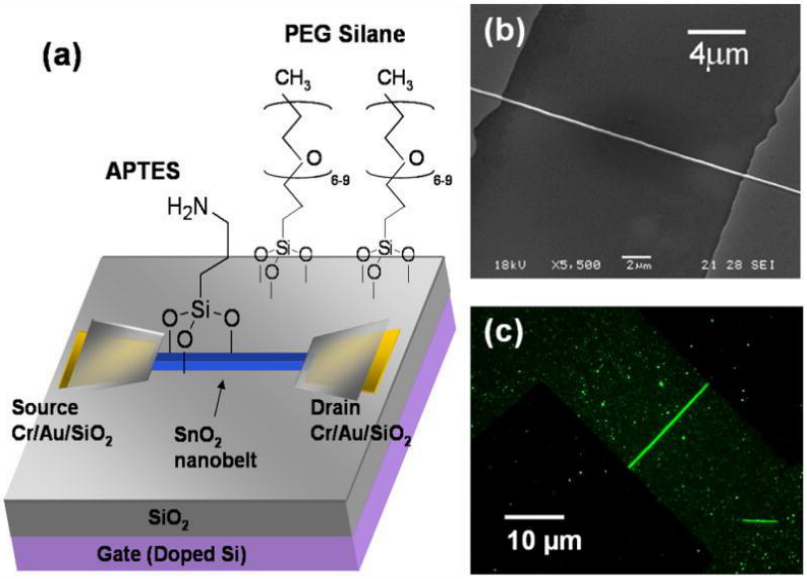

Figure A2. Schematic view of a nanobelt FET device (a) After PEG-silane passivation of SiO_2 and APTES functionalization of the SnO_2 channel to which streptavidin is bound. (b) SEM image of a SnO_2 nanobelt FET. (c) Fluorescence image of a SnO_2 nanobelt FET showing highly selective surface functionalization of the SnO_2 channel (Yi's 2008 paper).

This work was supported by NSF NIRT Grant No. ECS-0210332 and NIH GM 079592. From it came our July 2011 paper published in Biosensors and Bioelectronics entitled, “Functionalized SnO_2 nanobelt field-effect transistor sensors for label-free detection of cardiac troponin.” [106] As a MARTECH fellow, funding for my participation was also provided by FSU’s Center for Materials Research and Technology for our prososal, "Nanomechanical Assays for Detection of Atlered Protein Function in Cardiomyopathies".

APPENDIX B

USE OF VERTEBRATE ANIMALS

Skeletal myosin and actin will be purifiedfrom muscle tissue from adult New Zealand White rabbits. An initial estimate of approximately 4-5 rabbits will be required over the duration of the experiments proposed. Rabbits are procured by Laboratory Animal Resources (LAR) personnel and housed in the LAR facility. LAR personnel provide routine veterinary care where handling conforms to the current NIH/NRC*Guide for the Care and Use of Laboratory Animals*.

Use of animal tissues is necessary for these experiments as it is currently the only source from which to obtain ample quantities of purified skeletal myosin and, until recently, actin. Rabbit skeletal muscle is used because of its general similarity to that of humans and because of extensive knowledge already available about rabbit skeletal muscle function in its normal (non-diseased) condition. Lower vertebrate and invertebrate muscle, showing greater difference from human muscle in structure and protein composition and sequence, are thus not appropriate tissue sources for these experiments.

Rabbits are anesthetized by intramuscular injection (quadriceps) with a cocktail of at least 3 mg acepromazine + 10 mg/kg xylazine + 50 mg/kg of ketamine with adjustments as needed. Upon verifying surgical depth of anesthesia, the animal is exsanguinated in accordance with the Panel on Euthanasia of the American Veterinary Medical Association. The euthanized rabbit is skinned, viscera removed, and chilled with packed ice for approximately 15 minutes prior to tissue removal and subsequent protein purification as described above.

All procedures for ensuring avoidance of discomfort, distress, pain have been reviewed by staff veterinarians of the FSU Laboratory of Animal Resources facility (LAR), and approved by FSU's Animal Care and Use Committee. Lab personnel who handle animals receive required training, and non-survival surgeries to harvest muscle tissue are performed in the LAR necropsy room, with all animals surgically anesthetized for any procedure that might cause pain or distress as described above.

REFERENCES

1. Mogensen, J., et al., *Frequency and clinical expression of cardiac troponin I mutations in 748 consecutive families with hypertrophic cardiomyopathy.* J Am Coll Cardiol, 2004. **44**(12): p. 2315-25.

2. Kimura, A., et al., *Mutations in the cardiac troponin I gene associated with hypertrophic cardiomyopathy.* Nat Genet, 1997. **16**(4): p. 379-82.

3. Lang, R., et al., *Functional analysis of a troponin I (R145G) mutation associated with familial hypertrophic cardiomyopathy.* J Biol Chem, 2002. **277**(14): p. 11670-8.

4. Gomes, A.V. and J.D. Potter, *Molecular and cellular aspects of troponin cardiomyopathies.* Ann N Y Acad Sci, 2004. **1015**: p. 214-24.

5. Kohler, J., et al., *Familial hypertrophic cardiomyopathy mutations in troponin I (K183D, G203S, K206Q) enhance filament sliding.* Physiol Genomics, 2003. **14**(2): p. 117-28.

6. Tardiff, J.C., *Thin filament mutations: developing an integrative approach to a complex disorder.* Circ Res. **108**(6): p. 765-82.

7. Willott, R.H., et al., *Mutations in Troponin that cause HCM, DCM AND RCM: What can we learn about Thin Filament Function?* J Mol Cell Cardiol, 2009.

8. Watkins, H., H. Ashrafian, and C. Redwood, *Inherited cardiomyopathies.* N Engl J Med. **364**(17): p. 1643-56.

9. Brunet NM, et al., *Micromechanical thermal assays of Ca^{2+}-regulated thin-filament function and modulation by hypertrophic cardiomyopathy mutants of human cardiac troponin.* Journal of Biomedicine and Biotechnology, 2012.

10. Bloemink, M.J. and M.A. Geeves, *Shaking the myosin family tree: biochemical kinetics defines four types of myosin motor.* Semin Cell Dev Biol. **22**(9): p. 961-7.

11. Morano, I., et al., *Changes in essential myosin light chain isoform expression provide a molecular basis for isometric force regulation in the failing human heart.* J Mol Cell Cardiol, 1997. **29**(4): p. 1177-87.

12. Houdusse, A. and H.L. Sweeney, *Myosin motors: missing structures and hidden springs.* Curr Opin Struct Biol, 2001. **11**(2): p. 182-94.

13. Fajer, P.G., et al., *Myosin cleft closure by double electron–electron resonance and dipolar EPR.* Journal of Physics: Condensed Matter, 2007. **19**(28).

14. Pollard, T.D., *Cytoplasmic contractile proteins.* J Cell Biol, 1981. **91**(3 Pt 2): p. 156s-165s.

15. Davis, J.S., *A model for length-regulation in thick filaments of vertebrate skeletal myosin.* Biophys J, 1986. **50**(3): p. 417-22.

16. Winegrad, S., *Cardiac myosin binding protein C.* Circ Res, 1999. **84**(10): p. 1117-26.

17. Luther, P.K., et al., *Direct visualization of myosin-binding protein C bridging myosin and actin filaments in intact muscle.* Proc Natl Acad Sci U S A. **108**(28): p. 11423-8.

18. Boheler, K.R., et al., *Skeletal actin mRNA increases in the human heart during ontogenic development and is the major isoform of control and failing adult hearts.* J Clin Invest, 1991. **88**(1): p. 323-30.

19. Clark, K.A., et al., *Striated muscle cytoarchitecture: an intricate web of form and function.* Annu Rev Cell Dev Biol, 2002. **18**: p. 637-706.

20. Clement, S., et al., *Expression and function of alpha-smooth muscle actin during embryonic-stem-cell-derived cardiomyocyte differentiation.* J Cell Sci, 2007. **120**(Pt 2): p. 229-38.

21. Wang, F., et al., *Facilitated Cross-Bridge Interactions with Thin Filaments by Familial Hypertrophic Cardiomyopathy Mutations in alpha-Tropomyosin.* J Biomed Biotechnol. **2011**: p. 435271.

22. Palm, T., et al., *Disease-causing mutations in cardiac troponin T: identification of a critical tropomyosin-binding region.* Biophys J, 2001. **81**(5): p. 2827-37.

23. Perry, S.V., *Vertebrate tropomyosin: distribution, properties and function.* J Muscle Res Cell Motil, 2001. **22**(1): p. 5-49.

24. Takeda, S., et al., *Structure of the core domain of human cardiac troponin in the $Ca^{(2+)}$-saturated form.* Nature, 2003. **424**(6944): p. 35-41.

25. Vinogradova, M.V., et al., *$Ca^{(2+)}$-regulated structural changes in troponin.* Proc Natl Acad Sci U S A, 2005. **102**(14): p. 5038-43.

26. Pearlstone, J.R. and L.B. Smillie, *The interaction of rabbit skeletal muscle troponin-T fragments with troponin-I.* Can J Biochem Cell Biol, 1985. **63**(3): p. 212-8.

27. Kowlessur, D. and L.S. Tobacman, *Troponin regulatory function and dynamics revealed by H/D exchange-mass spectrometry.* J Biol Chem. **285**(4): p. 2686-94.

28. Bou-Assaf, G.M., et al., *Complexation and Calcium-Induced Conformational Changes in the Cardiac Troponin Complex Monitored by Hydrogen/Deuterium Exchange and FT-ICR Mass Spectrometry.* Int J Mass Spectrom. **302**(1-3): p. 116-124.

29. Herzberg, O. and M.N. James, *Structure of the calcium regulatory muscle protein troponin-C at 2.8 A resolution.* Nature, 1985. **313**(6004): p. 653-9.

30. Sundaralingam, M., et al., *Molecular structure of troponin C from chicken skeletal muscle at 3-angstrom resolution.* Science, 1985. **227**(4689): p. 945-8.

31. Galinska-Rakoczy, A., et al., *Structural basis for the regulation of muscle contraction by troponin and tropomyosin.* J Mol Biol, 2008. **379**(5): p. 929-35.

32. Rarick, H.M., et al., *The C terminus of cardiac troponin I is essential for full inhibitory activity and Ca^{2+} sensitivity of rat myofibrils.* J Biol Chem, 1997. **272**(43): p. 26887-92.

33. Murakami, K., et al., *Structural basis for Ca^{2+}-regulated muscle relaxation at interaction sites of troponin with actin and tropomyosin.* J Mol Biol, 2005. **352**(1): p. 178-201.

34. Pirani, A., et al., *Single particle analysis of relaxed and activated muscle thin filaments.* J Mol Biol, 2005. **346**(3): p. 761-72.

35. Blumenschein, T.M., et al., *Dynamics of the C-terminal region of TnI in the troponin complex in solution.* Biophys J, 2006. **90**(7): p. 2436-44.

36. Kowlessur, D. and L.S. Tobacman, *Troponin regulatory function and dynamics revealed by H/D exchange-mass spectrometry.* J Biol Chem, 2009.

37. Van Eyk, J.E., et al., *Distinct regions of troponin I regulate Ca^{2+}-dependent activation and Ca^{2+} sensitivity of the acto-S1-TM ATPase activity of the thin filament.* J Biol Chem, 1997. **272**(16): p. 10529-37.

38. Narita, A., et al., *$Ca^{(2+)}$-induced switching of troponin and tropomyosin on actin filaments as revealed by electron cryo-microscopy.* J Mol Biol, 2001. **308**(2): p. 241-61.

39. Galinska, A., et al., *The C terminus of cardiac troponin I stabilizes the Ca^{2+}-activated state of tropomyosin on actin filaments.* Circ Res. **106**(4): p. 705-11.

40. Foster, D.B., et al., *C-terminal truncation of cardiac troponin I causes divergent effects on ATPase and force: implications for the pathophysiology of myocardial stunning.* Circ Res, 2003. **93**(10): p. 917-24.

41. Klabunde, R.E., *Cardiovascular Physiology Concepts*. 2nd ed. 2011, Philadelphia: Lippincott Williams & Wilkins. 256.

42. Bers, D.M., *Calcium fluxes involved in control of cardiac myocyte contraction.* Circ Res, 2000. **87**(4): p. 275-81.

43. Varian, K.D., S. Raman, and P.M. Janssen, *Measurement of myofilament calcium sensitivity at physiological temperature in intact cardiac trabeculae.* Am J Physiol Heart Circ Physiol, 2006. **290**(5): p. H2092-7.

44. Potter, J.D. and J. Gergely, *Troponin, tropomyosin, and actin interactions in the Ca^{2+} regulation of muscle contraction.* Biochemistry, 1974. **13**(13): p. 2697-703.

45. Gordon, A.M., E. Homsher, and M. Regnier, *Regulation of contraction in striated muscle.* Physiol Rev, 2000. **80**(2): p. 853-924.

46. Parry, D.A. and J.M. Squire, *Structural role of tropomyosin in muscle regulation: analysis of the x-ray diffraction patterns from relaxed and contracting muscles.* J Mol Biol, 1973. **75**(1): p. 33-55.

47. Huxley, H.E., *Muscular contraction and cell motility.* Nature, 1973. **243**(5408): p. 445-9.

48. Vibert, P., R. Craig, and W. Lehman, *Steric-model for activation of muscle thin filaments.* J Mol Biol, 1997. **266**(1): p. 8-14.

49. Xu, C., et al., *Tropomyosin positions in regulated thin filaments revealed by cryoelectron microscopy.* Biophys J, 1999. **77**(2): p. 985-92.

50. Gordon, A.M., M. Regnier, and E. Homsher, *Skeletal and cardiac muscle contractile activation: tropomyosin "rocks and rolls".* News Physiol Sci, 2001. **16**: p. 49-55.

51. McKillop, D.F. and M.A. Geeves, *Regulation of the interaction between actin and myosin subfragment 1: evidence for three states of the thin filament.* Biophys J, 1993. **65**(2): p. 693-701.

52. Van Dijk, J., et al., *Characterization of three regulatory states of the striated muscle thin filament.* J Mol Biol, 2002. **323**(3): p. 475-89.

53. Gordon, A.M., et al., *Skeletal muscle regulatory proteins enhance F-actin in vitro motility.* Adv Exp Med Biol, 1998. **453**: p. 187-96; discussion 196-7.

54. Gordon, A.M., et al., *Calcium regulation of skeletal muscle thin filament motility in vitro.* Biophys J, 1997. **72**(3): p. 1295-307.

55. Howard, J., A.J. Hunt, and S. Baek, *Assay of microtubule movement driven by single kinesin molecules.* Methods Cell Biol, 1993. **39**: p. 137-47.

56. Regnier, M., et al., *Thin filament near-neighbour regulatory unit interactions affect rabbit skeletal muscle steady-state force-$Ca^{(2+)}$ relations.* J Physiol, 2002. **540**(Pt 2): p. 485-97.

57. Huxley, A.F., *Muscle structure and theories of contraction.* Prog Biophys Biophys Chem, 1957. **7**: p. 255-318.

58. Rayment, I., et al., *Structure of the actin-myosin complex and its implications for muscle contraction.* Science, 1993. **261**(5117): p. 58-65.

59. Rayment, I., et al., *Three-dimensional structure of myosin subfragment-1: a molecular motor.* Science, 1993. **261**(5117): p. 50-8.

60. Schroder, R.R., et al., *Three-dimensional atomic model of F-actin decorated with Dictyostelium myosin S1.* Nature, 1993. **364**(6433): p. 171-4.

61. Schoenberg, M., et al., *Cross-bridge attachment in relaxed muscle.* Adv Exp Med Biol, 1984. **170**: p. 269-84.

62. Ebashi, S. and M. Endo, *Calcium ion and muscle contraction.* Prog Biophys Mol Biol, 1968. **18**: p. 123-83.

63. Hellam, D.C. and R.J. Podolsky, *Force measurements in skinned muscle fibres.* J Physiol, 1969. **200**(3): p. 807-19.

64. Julian, F.J., *Activation in a skeletal muscle contraction model with a modification for insect fibrillar muscle.* Biophys J, 1969. **9**(4): p. 547-70.

65. Donaldson, S.K. and W.G. Kerrick, *Characterization of the effects of Mg^{2+} on Ca^{2+}- and Sr^{2+}-activated tension generation of skinned skeletal muscle fibers.* J Gen Physiol, 1975. **66**(4): p. 427-44.

66. Walker, J.S., X. Li, and P.M. Buttrick, *Analysing force-pCa curves.* J Muscle Res Cell Motil. **31**(1): p. 59-69.

67. Lindhout, D.A., et al., *The role of electrostatics in the interaction of the inhibitory region of troponin I with troponin C.* Biochemistry, 2005. **44**(45): p. 14750-9.

68. Teare, D., *Asymmetrical hypertrophy of the heart in young adults.* Br Heart J, 1958. **20**(1): p. 1-8.

69. Tardiff, J.C., *Sarcomeric proteins and familial hypertrophic cardiomyopathy: linking mutations in structural proteins to complex cardiovascular phenotypes.* Heart Fail Rev, 2005. **10**(3): p. 237-48.

70. Geisterfer-Lowrance, A.A., et al., *A molecular basis for familial hypertrophic cardiomyopathy: a beta cardiac myosin heavy chain gene missense mutation.* Cell, 1990. **62**(5): p. 999-1006.

71. Du, J., et al., *Impaired relaxation is the main manifestation in transgenic mice expressing a restrictive cardiomyopathy mutation, R193H, in cardiac TnI.* Am J Physiol Heart Circ Physiol, 2008. **294**(6): p. H2604-13.

72. Mogensen, J., et al., *Idiopathic restrictive cardiomyopathy is part of the clinical expression of cardiac troponin I mutations.* J Clin Invest, 2003. **111**(2): p. 209-16.

73. Willott, R.H., et al., *Mutations in Troponin that cause HCM, DCM AND RCM: what can we learn about thin filament function?* J Mol Cell Cardiol. **48**(5): p. 882-92.

74. Sung, S.S., et al., *Mutations in genes encoding fast-twitch contractile proteins cause distal arthrogryposis syndromes.* Am J Hum Genet, 2003. **72**(3): p. 681-90.

75. Kimber, E., et al., *Distal Arthrogryposis: Clinical and Genetic Findings.* Acta Paediatr.

76. Robinson, P., et al., *Mutations in fast skeletal troponin I, troponin T, and beta-tropomyosin that cause distal arthrogryposis all increase contractile function.* Faseb J, 2007. **21**(3): p. 896-905.

77. Shrimpton, A.E. and J.J. Hoo, *A TNNI2 mutation in a family with distal arthrogryposis type 2B.* Eur J Med Genet, 2006. **49**(2): p. 201-6.

78. Rarick, H.M., et al., *Interactions at the NH2-terminal interface of cardiac troponin I modulate myofilament activation.* J Mol Cell Cardiol, 1999. **31**(2): p. 363-75.

79. Sykes, B.D., *Pulling the calcium trigger.* Nat Struct Biol, 2003. **10**(8): p. 588-9.

80. Compton, L.A., et al., *Increased calcium sensitivity of actin filament sliding by FHC cardiac troponin I mutants D196N and S199N.* Biophys J, 2005. **88**(316a).

81. Kobayashi, T. and R.J. Solaro, *Increased Ca^{2+} affinity of cardiac thin filaments reconstituted with cardiomyopathy-related mutant cardiac troponin I.* J Biol Chem, 2006. **281**(19): p. 13471-7.

82. Homsher, E., F. Wang, and J. Sellers, *Factors affecting filament velocity in in vitro motility assays and their relation to unloaded shortening velocity in muscle fibers.* Adv Exp Med Biol, 1993. **332**: p. 279-89; discussion 289-90.

83. Liang, B., et al., *Ca^{2+} regulation of rabbit skeletal muscle thin filament sliding: role of cross-bridge number.* Biophys J, 2003. **85**(3): p. 1775-86.

84. Schoffstall, B., et al., *Ca^{2+} sensitivity of regulated cardiac thin filament sliding does not depend on myosin isoform.* J Physiol, 2006. **577**(Pt 3): p. 935-44.

85. Chase, P.B., et al., *Viscosity and solute dependence of F-actin translocation by rabbit skeletal heavy meromyosin.* Am J Physiol Cell Physiol, 2000. **278**(6): p. C1088-98.

86. Regnier, M., et al., *2-deoxy-ATP enhances contractility of rat cardiac muscle.* Circ Res, 2000. **86**(12): p. 1211-7.

87. Regnier, M., D.A. Martyn, and P.B. Chase, *Calmidazolium alters Ca^{2+} regulation of tension redevelopment rate in skinned skeletal muscle.* Biophys J, 1996. **71**(5): p. 2786-94.

88. Mariano, A.C., et al., *Dimethyl sulphoxide enhances the effects of P(i) in myofibrils and inhibits the activity of rabbit skeletal muscle contractile proteins.* Biochem J, 2001. **358**(Pt 3): p. 627-36.

89. Solaro, R.J. and H.M. Rarick, *Troponin and tropomyosin: proteins that switch on and tune in the activity of cardiac myofilaments.* Circ Res, 1998. **83**(5): p. 471-80.

90. Yang, Z., et al., *Differences between cardiac and skeletal troponin interaction with the thin filament probed by troponin exchange in skeletal myofibrils.* Biophys J, 2009. **97**(1): p. 183-94.

91. Kron, S.J., et al., *Assays for actin sliding movement over myosin-coated surfaces.* Methods Enzymol, 1991. **196**: p. 399-416.

92. Margossian, S.S. and S. Lowey, *Preparation of myosin and its subfragments from rabbit skeletal muscle.* Methods Enzymol, 1982. **85 Pt B**: p. 55-71.

93. Pardee, J.D. and J.A. Spudich, *Purification of muscle actin.* Methods Cell Biol, 1982. **24**: p. 271-89.

94. Ruiz-Opazo, N. and B. Nadal-Ginard, *Alpha-tropomyosin gene organization. Alternative splicing of duplicated isotype-specific exons accounts for the production of smooth and striated muscle isoforms.* J Biol Chem, 1987. **262**(10): p. 4755-65.

95. Gill, S.C. and P.H. von Hippel, *Calculation of protein extinction coefficients from amino acid sequence data.* Anal Biochem, 1989. **182**(2): p. 319-26.

96. Schoffstall, B., et al., *Effects of rapamycin on cardiac and skeletal muscle contraction and crossbridge cycling.* J Pharmacol Exp Ther, 2005. **312**(1): p. 12-8.

97. Li, M.X., L. Spyracopoulos, and B.D. Sykes, *Binding of cardiac troponin-I147-163 induces a structural opening in human cardiac troponin-C.* Biochemistry, 1999. **38**(26): p. 8289-98.

98. Sellers, J.R., et al., *Myosin-specific adaptations of the motility assay.* Methods Cell Biol, 1993. **39**: p. 23-49.

99. Homsher, E., et al., *Calcium regulation of thin filament movement in an in vitro motility assay.* Biophys J, 1996. **70**(4): p. 1881-92.

100. Homsher, E., F. Wang, and J.R. Sellers, *Factors affecting movement of F-actin filaments propelled by skeletal muscle heavy meromyosin.* Am J Physiol, 1992. **262**(3 Pt 1): p. C714-23.

101. Sternberg, S.R., *Biomedical Image Processing.* IEEE Computer, 1983. **16**: p. 23-34.

102. Van Eyk, J.E. and R.S. Hodges, *The biological importance of each amino acid residue of the troponin I inhibitory sequence 104-115 in the interaction with troponin C and tropomyosin-actin.* J Biol Chem, 1988. **263**(4): p. 1726-32.

103. Tobacman, L.S., et al., *The troponin tail domain promotes a conformational state of the thin filament that suppresses myosin activity.* J Biol Chem, 2002. **277**(31): p. 27636-42.

104. Homsher, E., et al., *Regulatory proteins alter nucleotide binding to acto-myosin of sliding filaments in motility assays.* Biophys J, 2003. **85**(2): p. 1046-52.

105. Higashe-Fujime, S. and T. Hozumi, *The mechanism for mechanochemical energy transduction in actin-myosin interaction revealed by in vitro motility assay with ATP analogs.* Biochemical and Biophysical Research Communications, 1996. **221**: p. 773-778.

106. Cheng, Y., et al., *Functionalized SnO_2 nanobelt field-effect transistor sensors for label-free detection of cardiac troponin.* Biosens Bioelectron. **26**(11): p. 4538-44.

BIOGRAPHICAL SKETCH

The author was born in Oak Ridge, New Jersey in 1975 and attended high school and college in Florida. She received her B.S in Biology in 1997 from the Florida State University. She began her graduate studies in the Florida State University Molecular Biophysics program in 2004, but was later transferred to the Departmant of Biology from which she received the present M.S. in Summer of 2012, two years after her departure. In the interim, Ms. Meyer was employed as a senior research assistant in a structural biology lab at Oregon Health and Science University in Portland, Oregon, where she currently still works and resides.